Journal of South American Earth Sciences 96 (2019) 102384

Contents lists available at ScienceDirect

Journal of South American Earth Sciences

journal homepage: www.elsevier.com/locate/jsames

Early to late Neoproterozoic subduction-accretion episodes in the Cariris Velhos Belt of the Borborema Province, Brazil: Insights from isotope and whole-rock geochemical data of supracrustal and granitic rocks

Lauro Cézar M. de Lira Santos[a,b,*], Elton L. Dantas[a], Peter A. Cawood[c], Geysson de A. Lages[d], Haroldo M. Lima[e], Edilton J. dos Santos[d,1], Fabrício A. Caxito[f]

[a] Departamento de Geologia, Universidade Federal de Pernambuco, Brazil
[b] Instituto de Geociências, Universidade de Brasília, Brazil
[c] School of Earth, Atmosphere and Environment, Monash University, Australia
[d] Serviço Geológico do Brasil - CPRM, Brazil
[e] Departamento de Geologia, Universidade Federal do Ceará, Brazil
[f] CPMTC, Instituto de Geociências, Universidade Federal de Minas Gerais, Brazil

ARTICLE INFO

Keywords:
Early Neoproterozoic post-orogenic setting
Ediacaran granitic magmatism
Cariris Velhos and Brasiliano orogens
Borborema Province
West Gondwana

ABSTRACT

The Cariris Velhos Belt is an unique domain of the Borborema Province, Brazil, because it presents magmatic and metamorphic lithotectonic associations spanning all the Neoproterozoic. In this study, we investigate the main sources of its major supracrustal sequence (*i.e.* São Caetano Complex) as well as genetic aspects of a later intrusive granitic body, the São Pedro Stock. Detrital U-Pb zircon determinations for the supracrustal rocks are characterized by a major peak in the range of 1.0-0.9 Ga, with maximum deposition age at around 0.86 Ga. Minor components are aged at 1.8-1.6 Ga and 2.5 Ga. The Nd isotopic composition for this unit suggest crustal reworking of Meso-to Paleoproterozoic sources as well as inheritance of juvenile mantle material. Whole-rock geochemical data points out to derivation from magmatic arc-related andesites and rhyolites as well as foreland material, and we interpret this sequence as remnant of the Cariris Velhos (1.0-0.9 Ga) post-orogenic basin. The São Pedro Stock corresponds to a mostly isotropic intrusion of dominantly granitic composition. U-Pb zircon data from a monzogranitic and a tonalitic samples suggest crystallization ages of *ca.* 615 ± 02 Ma and 596 ± 22 Ma, respectively. Zircon crystals with ages of ca. 981 ± 29 Ma are interpreted as inherited crystals. Sm-Nd isotopic behavior is similar from samples of the São Caetano Complex, whereas overall geochemistry suggests crystallization from high-K calc-alkaline and peraluminous magmas, in addition to trace-element distribution compatible with Cordilleran granites. It is proposed that the São Pedro stock were formed in a modern-style subduction zone in later stages of the Brasiliano-Pan African orogeny (0.6-0.5 Ga). Accordingly, we conclude that systematic subduction-accretion episodes took place in this part of West Gondwana from early to late Neoproterozoic times.

1. Introduction

The preserved lithotectonic record of convergent plate boundaries provide clues to unravel several stages of interaction between subducting lithosphere, adjoining mantle wedge and adjacent terranes (Tatsumi, 2005; Cawood et al., 2009; Li et al., 2010). For instance, it is assumed that modern accretionary and collisional belts (*e.g.* West Pacific margin and the Alpine-Himalayan chain) are characterized by specific volcano-plutonic and metamorphic assemblages that are considered models for Proterozoic orogenies (*e.g.* Stern, 2005; Cawood et al., 2009; Sizova et al., 2010; Brown and Johnson, 2018). In spite of systematic episodes of crustal reworking, advances in geochemical and isotopic analysis have greatly improved our knowledge on the evolution of Archean and Proterozoic orogens (*e.g.* Tatsumi and Kogiso, 2003; Sizova et al., 2010; Cawood et al., 2013; Gerya, 2014; Wang et al., 2017).

The Borborema Province (BP) in northeastern Brazil occupies a key spatial and temporal position in West Gondwana, linking with highly

* Corresponding author. Departamento de Geologia, Universidade Federal de Pernambuco, Brazil.
E-mail address: lauromontefalco@gmail.com (L.C.M.d.L. Santos).
[1] In Memoriam.

https://doi.org/10.1016/j.jsames.2019.102384
Received 19 May 2019; Received in revised form 6 October 2019; Accepted 6 October 2019
Available online 11 October 2019
0895-9811/

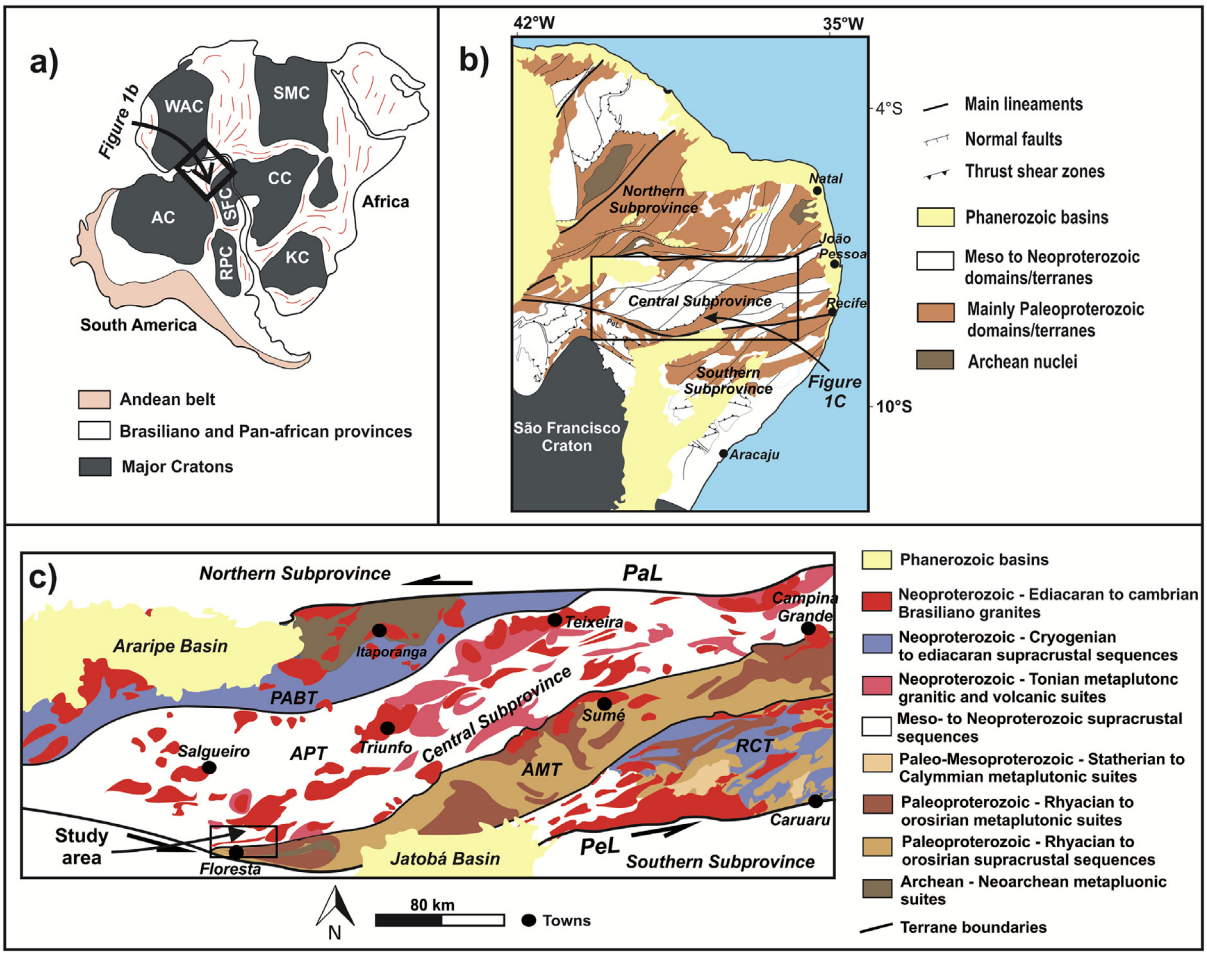

Fig. 1. a) Geodynamic context of the Borborema Province in a simplified pre-drift reconstruction of West Africa and northeastern South America, b) Tectonic framework of the Borborema Province and c) Schematic geological map of the Central Subprovince and its terranes with the study area highlighted.

deformed african mobile belts that record tectonic episodes spanning most of the Precambrian (Brito Neves et al., 2000; Neves, 2003; Van Schmus et al., 2008, 2011). This province is characterized by a complex structural and lithostratigraphic framework, resulting in a variety of geodynamic interpretations, including: i) accretion of exotic terranes, similar to the western North American Cordillera (Santos, 1995; Brito Neves et al., 2000; Santos et al., 2017a, 2018); ii) reworking of early Paleoproterozoic crust in an Ediacaran intracontinental orogen (Neves, 2015); and, iii) different stages of the Wilson cycle, involving rifting, drifting, subduction and continent-continent collision (Oliveira et al., 2010; Ganade de Araujo et al., 2014a; Caxito et al., 2014a, 2014b, 2016).

One of the main features of the province is the abundance of Neoproterozoic granites associated with the Brasiliano-Pan African orogeny (~0.60-0.50 Ga; Brito Neves et al., 2014 and references therein). They form large batholiths, stocks and plutons that have been the main focus of study for decades (*e.g.* Santos and Medeiros, 1999; Guimarães and Silva Filho, 2000; Ferreira et al., 2003; Neves et al., 2003; Sial and Ferreira, 2015; Amorim et al., 2018). However, the role of metasedimentary sequences in the evolution of the province has only recently been emphasized, including the investigation of probable sources, depositional settings and tectonic significance of paleobasins (*e.g.* Oliveira et al., 2015; Arthaud et al., 2015; Caxito et al., 2014c, 2016; Lima et al., 2019; Basto et al., 2019). In spite of paleoproterozoic source contributions, provenance studies in other portions of Gondwana have shown that major supracrustal sequences provide a wide range of Neoproterozoic deposition ages (*i.e.* 1000 - 590 Ma), marking the development of distinct tectonic settings, including rift systems, passive margins and arc-related basins (Jöns and Schenk, 2008; De Wit et al., 2008; Van Schmus et al., 2008; Nascimento et al., 2015).

Within the central Borborema Province, the Alto Pajeú Terrane (APT) hosts a number of Brasiliano-related granites that are mostly intrusive into early Neoproterozoic metasedimentary and metavolcanic sequences. This terrane is considered the type area of the Cariris Velhos tectonic event (ca. 1.0–0.96 Ga), also known as the Cariris Velhos Belt (CVB). Two hypotheses are proposed for the origin of this belt: i) Accretion-collision setting with the formation of continental magmatic arcs and ophiolite emplacement (Kozuch, 2003; Santos et al., 2010; Caxito et al., 2014a; Lages and Dantas, 2016); and, ii) Rift-related setting and reworking of a stabilized Paleoproterozoic crust (Guimarães et al., 2012, 2015).

In the CVB as well as in the rest of central Borborema Province, granitic suites are mostly intrusive into supracrustal sequences that have a range of depositional ages and experienced variable metamorphic P-T-t conditions (Santos and Medeiros, 1999; Santos et al., 2004; Neves et al., 2017). The granites have been structurally interpreted as early-, syn and post-kinematic according to the relationships with major shear zones, spanning from 650 to 512 Ma and classified as belonging to the calc-alkaline, shoshonitic and A-type series (Guimarães et al., 2011; Van Schmus et al., 2011). However, the current knowledge of the Brasiliano related granites and their tectonic setting in the CVB are limited in a wider context of West Gondwana reconstruction (see Santos and Medeiros, 1999 and Brito Neves et al., 2014 for details).

In this paper, we present the results of integrated field mapping, petrography, U-Pb zircon data, and whole-rock geochemistry and Sm-Nd systematics on metasedimentary rocks of the São Caetano Complex

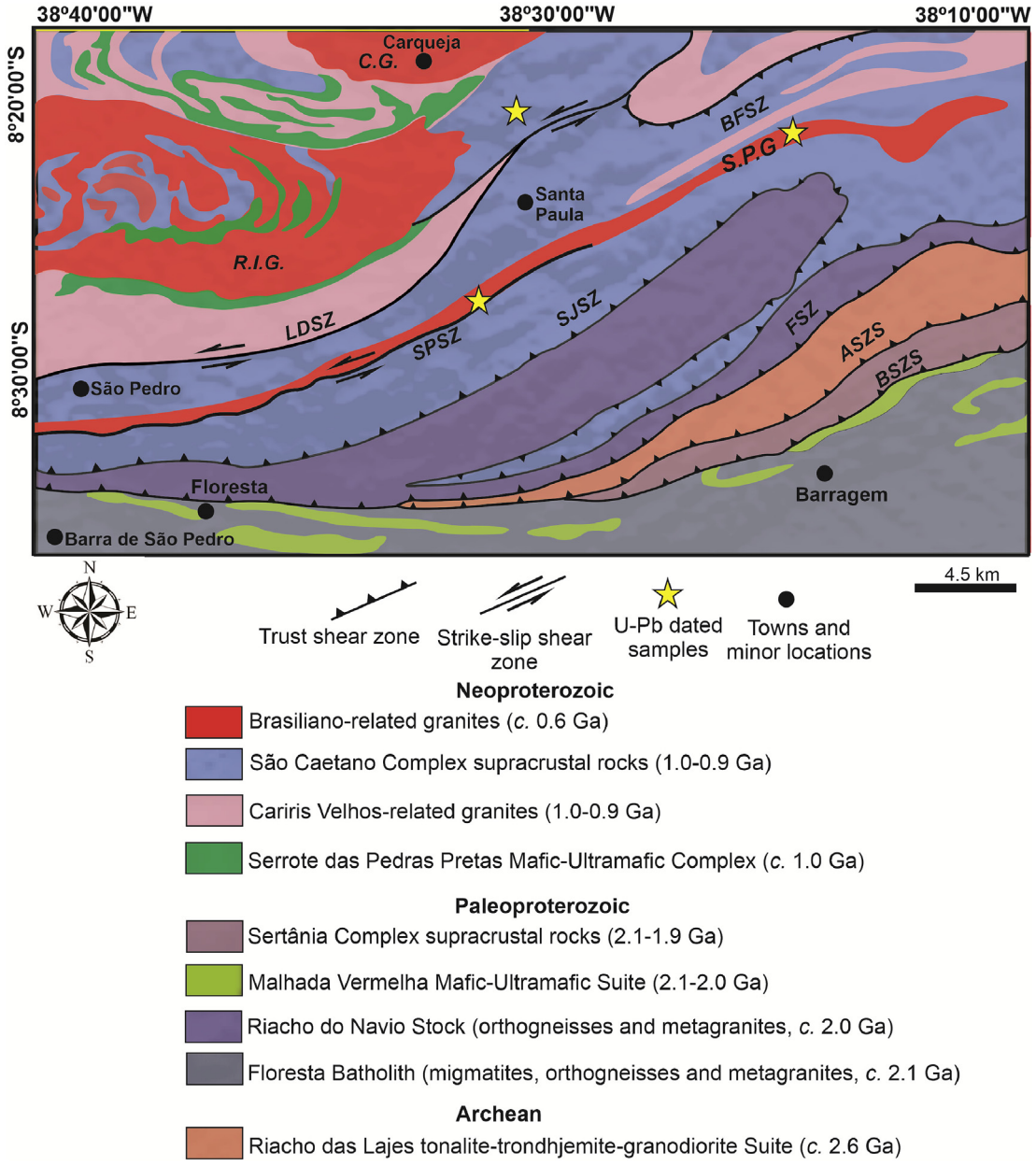

Fig. 2. Simplified geological map of the studied region and location of the U-Pb zircon dated samples. S.P.G. = São Pedro granite; C.G. = Carqueja granite; R.I.C. = Riacho do Icó granite; LDZ = Lagoa do Defunto Shear Zone; BFZ = Barra de Forquilha Shear Zone; SPZ = São Pedro Shear Zone; SJSZ = Serra de Jabitacá Shear Zone; FSZ = Floresta Shear Zone; ASZ = Airí Shear Zone; BSZ = Barragem Shear Zone.

(SCC) and the intrusive granitic São Pedro Stock (SPS) in the Floresta region, Pernambuco. Our data enable an assessment of the Neoproterozoic evolution of Borborema Province and its role in the evolution of central West Gondwana.

2. Geological setting

2.1. Borborema Province

The Borborema Province constitutes the northeastern portion of the Precambrian South American platform (Almeida et al., 1981) and in West Gondwana reconstructions, can be traced into West Africa through Benin, Nigeria and Cameroon (Fig. 1a; Van Schmus et al., 2008; Ganade de Araújo et al., 2016). It is bounded to the south by the São Francisco Craton, to the west by the Parnaíba Basin, and to the north and east by marginal Phanerozoic basins. It is formed by highly deformed and frequently migmatized Paleoproterozoic basement domains/terranes, locally including Archean fragments (Brito Neves et al., 2000; Fetter et al., 2000; Van Schmus et al., 2008; Dantas et al., 2013; Santos et al., 2015a,b, 2017b; Costa et al., 2015, 2018). The basement sequences are unconformably overlain by early to late Neoproterozoic metavolcano-sedimentary (mostly metapelitic) belts (Van Schmus et al., 2003; Hollanda et al., 2015) that are intruded by granites, the earliest of which, of late Cryogenian – early Ediacaran age, interpreted as remnants of continental magmatic arcs (Santos and Medeiros, 1999; Ganade de Araújo et al., 2014a; Brito Neves et al., 2014), followed by syn-to post-collisional and strike-slip related granitoids (*e.g.* Van Schmus et al., 2011; Caxito et al., 2016).

The province is structurally complex, being characterized by a network of shear zones up to several kilometers-wide (Archanjo et al., 2008; Oliveira and Medeiros, 2018; Cordani et al., 2013; Viegas et al., 2014, 2016), being divided into Northern, Central (or Transversal) and

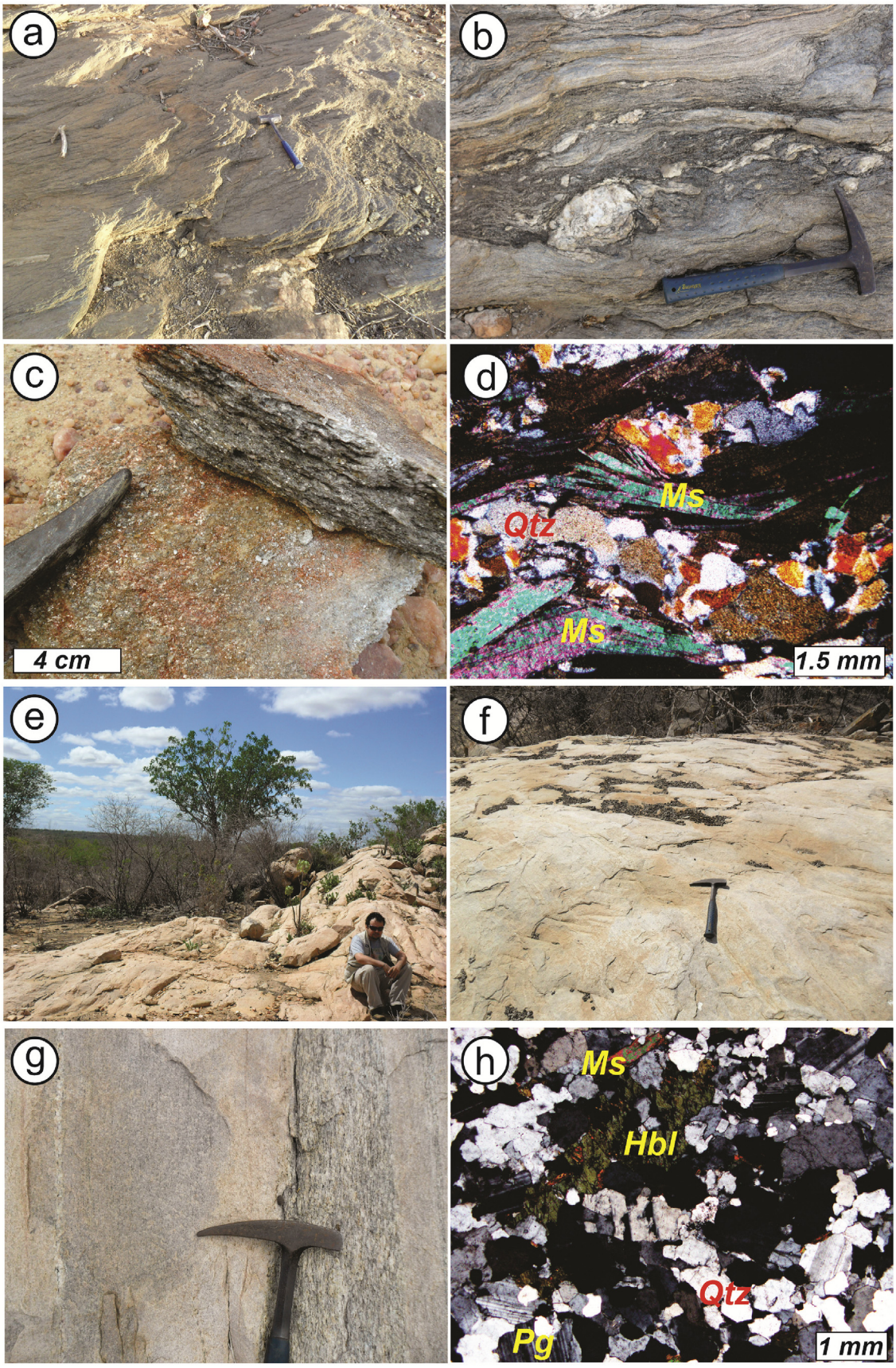

(caption on next page)

Fig. 3. Representative field and petrographic features of the studied rocks. São Caetano Complex: a) Shallow-dipping foliation on biotite-muscovite schist; b) Local quartz segregations exhibiting curvilinear shapes on mylonitic schist; c) Sample of muscovite-schist with planar-linear fabric of phyllosilicate lamellae alignment; d) Microfolds of muscovite lamellae along major foliation planes in muscovite-schist sample. São Pedro Stock: e) Pinkish isotropic monzogranite (Dated sample FL-89); f) Coarse-grained grayish granodiorite exhibiting incipient foliation; and, g) Contact between slightly foliated granodiorite and mylonites from the São Caetano Complex related to the São Pedro Shear Zone (dated sample FL-35B on the left side of the image); h) Hypidiomorphic granular texture on granodiorite sample exhibiting partial chloritization of a hornblende crystal.

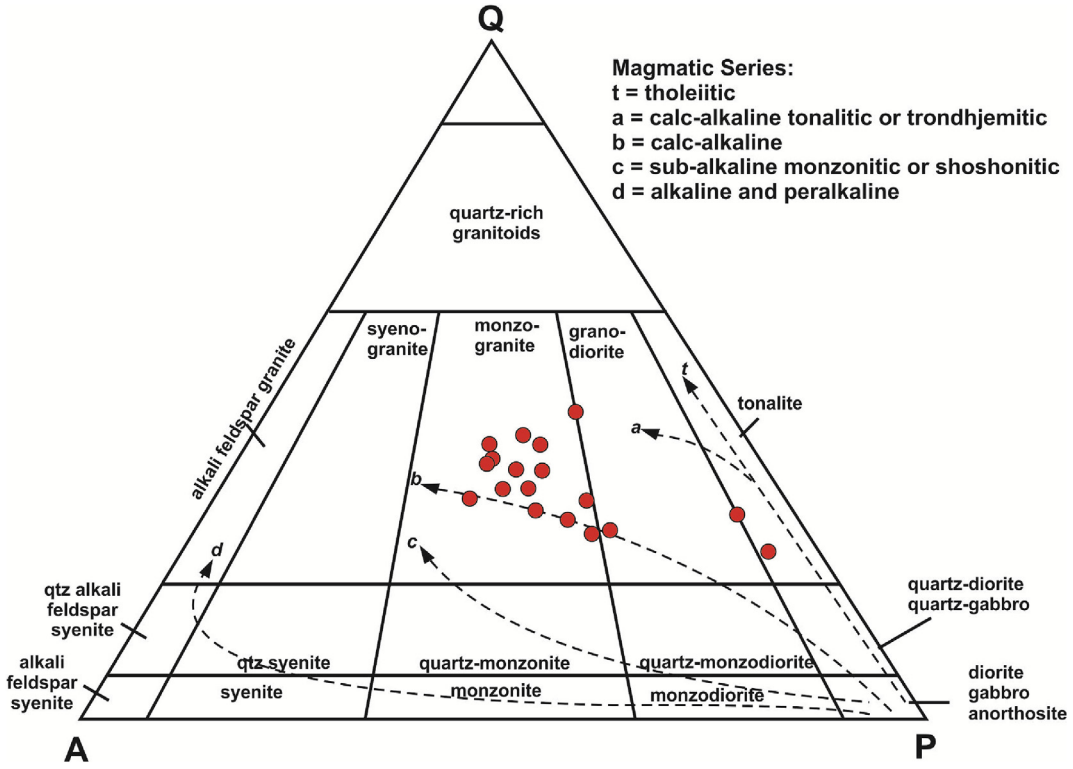

Fig. 4. Modal composition of studied samples from the São Pedro Stock plotted on the Q-A-P triangular diagram from Streckeisen (1976).

Southern subprovinces (Fig. 1b; Van Schmus et al., 1995, 2011; Santos and Medeiros, 1999; Brito Neves et al., 2000). The Central Subprovince comprises a complex mosaic of terranes (*i.e.* São José do Caiano, Piancó-Alto Brígida, Alto Pajeú, Alto Moxotó and Rio Capibaribe), delineated by NE-SW shear zones that are subsidiary of major E-W lineaments. It is assumed that these domains recorded several stages of accretion-collision tectonics and rifting that are marked by variable orthogneisses, supracrustal sequences and abundant metagranitic and granitic plutons (Fig. 1c; Santos and Medeiros, 1999; Brito Neves et al., 2000).

2.2. The Cariris Velhos Belt and the main geological features of the studied rocks

The overall northeast-southwest trending Cariris Velhos Belt is separated from the Piancó-Alto Brígida terrane to the northwest by the strike-slip NE-SW Serra do Caboclo sinistral shear zone, and from the Alto Moxotó Terrane by the Serra de Jabitacá thrust-fold system (Santos and Medeiros, 1999). This belt is interpreted as a short-lived (< 100 Ma) magmatic arc-system that was active during the early Neoproterozoic, related to the Cariris Velhos event (Kozuch, 2003; Santos et al., 2010; Caxito et al., 2014a; Lages and Dantas, 2016). This pulse of magmatic activity was firstly described by Brito Neves et al. (1995) and is responsible for the emplacement of numerous calc-alkaline and peraluminous Tonian andesites and granites (*ca.* 1.0-0.92 Ga), as well as the deposition of mature and immature pelitic metasedimentary and metavolcanoclastic rocks of the Riacho Gravatá and São Caetano complexes. These supracrustal sequences reached lower amphibolite facies, being subsequently intruded by several Brasiliano-related plutons (Santos et al., 2010). Continental extension is alternatively regarded as the main mechanism for the CVB development, including reworking of possible Paleoproterozoic (*c.* 2.2 and 1.9 Ga) crust between 806 Ma and 1091 Ma (Guimarães et al., 2012).

In the study area, the investigated units crop out near the tectonic contact between the CVB and the Alto Moxotó Terrane along the Serra de Jabitacá Shear Zone (Fig. 2). The main units of the Alto Moxotó terrane involve metaplutonic suites as well as supracrustal rocks that vary from Archean to Paleoproterozoic in age (Santos et al., 2017b). The dominant unit of the CVB is the São Caetano Complex, generally described as a heterogeneous metavolcano-sedimentary sequence, including metagraywackes, metapelites, metapsamites and metavolcanic and metavolcanoclastic rocks (Santos et al., 2010; Guimarães et al., 2012). Available geochronological data for the rocks of the São Caetano Complex in other areas of the belt yielded maximum deposition ages at around 932 Ma (Van Schmus et al., 2011) and 806–862 Ma (Guimarães et al., 2012). Chronocorrelated units include the Mafic-Ultramafic Serrote das Pedras Pretas Suite (SPP) (Lages and Dantas, 2016) and calc-alkaline metagranites, interpreted by Santos (1995) and Kozuch (2003) as associated with late Meso-to early Neoproterozoic plate convergence. The Carqueja, Riacho do Icó and São Pedro stocks are examples of late Neoproterozoic magmatic suites in the region.

Rocks of the São Caetano Complex were intensively affected by thrust and strike-slip shear zones, cropping out as low-dipping foliation on brownish grey schists (Fig. 3a), or strongly deformed planar-linear mylonites, exhibiting local quartz or quartz-feldspar segregations (Fig. 3b). Metavolcanic and metavolcanoclastic rocks are scarce and

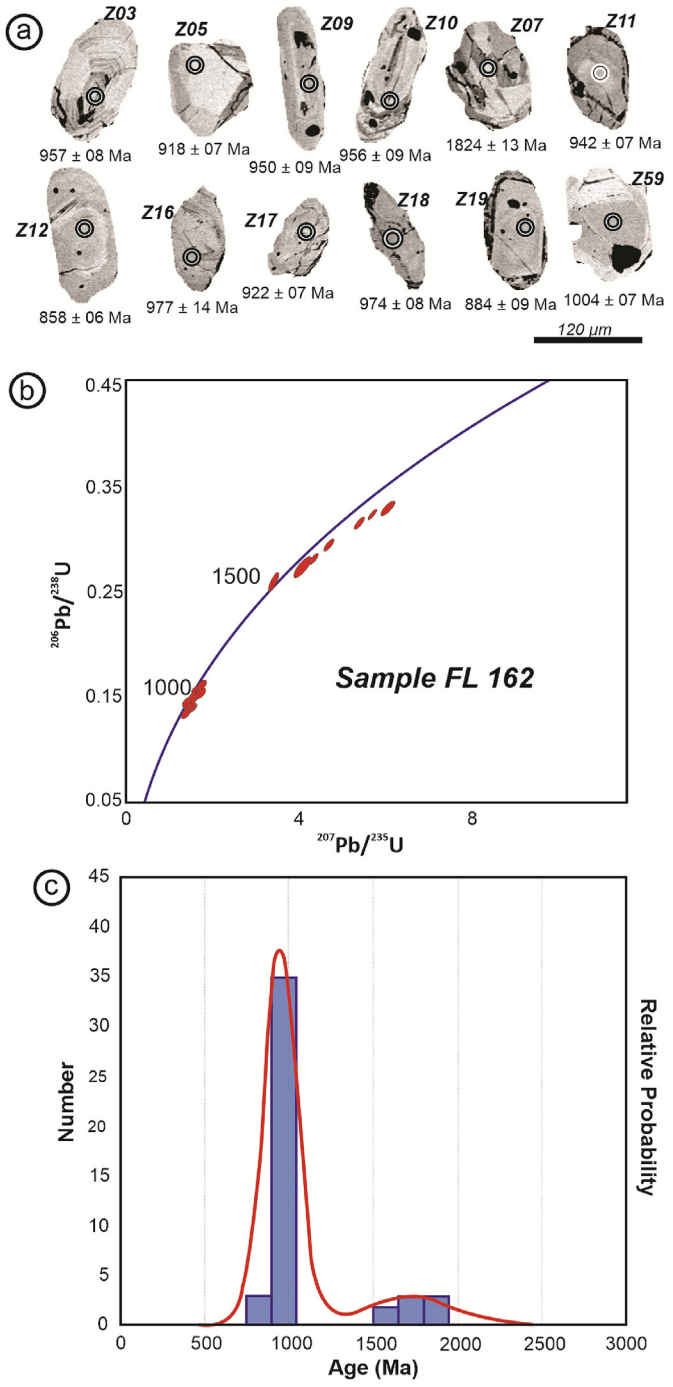

Fig. 5. Sample FL-162 (biotite-muscovite schist): a) Representative cathodoluminescence images of analyzed zircon crystals, b) Concordia diagram and c) frequency histogram and probability density curve.

occur as local intercalations within the biotite-muscovite schists. They form thick layers of coarse-grained amphibolites made up of dark greenish radial hornblende and grey plagioclase crystals, with minor clinopyroxene relics. In some portions, amphibolites exhibit minor inclusions of very-fine grain sized greenish layers with chlorite, epidote, calcite and actinolite. In such rocks, minor sericite inclusions are the result of plagioclase alteration. Metavolcanoclastic rocks may present obliterated breccia to lapilli textures, with mafic minerals replaced by clinozoisite and tremolite. Biotite-muscovite schists are characterized by aligned aggregates of coarse-grained phyllosilicates consisting of muscovite, biotite and minor chlorite (Fig. 3c). They have lepidoblastic texture and display ductile structural markers, including quartz ribbons with recrystallized rims and microfolds, mostly marked by bent muscovite crystals (Fig. 3d). Garnet might be present in a lesser extent and occur as hypidioblastic grains with descrete inner zoning, including tiny inclusions of rutile and ilmenite, whereas zircon crystals are mostly present along biotite lamellae. The overall metamorphic assemblage of the metavolcanic rocks is suggestive of greenschist metamorphic conditions, however, local migmatization on schists implicates that metamorphic peak reached high amphibolite facies, which is coherent with regional metamorphism described by Brito Neves et al. (2000).

The São Pedro Stock is mostly underformed and contains a series of fine-to coarse grained, grayish to pink to pale grey granitoids, lacking any evidence of mafic enclaves or xenoliths (Fig. 3e and f). The contact with the host rocks of the São Caetano Complex is generally abrupt; however, this stock is partially affected by the strike-slip sinistral São Pedro Shear Zone, producing mylonitic contacts along its southern margin (Fig. 3g). The studied samples have a hypidiomorphic to allotriomorphic granular texture (Fig. 3h), and are characterized by similar proportions of quartz and plagioclase (40%), whereas microcline crystals represent 10–20% of the rock composition. Quartz crystals are subhedric to anhedric and compose a homogeneous and underformed groundmass; however, some grains may exhibit undulose extinction and evidence for subgrain rotation. Plagioclase crystals are subhedric and exhibit mymerkitic intergrowth relicts and curvilinear contacts with quartz and microcline. Zoned plagioclase crystals can also be present, whereas the few muscovite crystals form intersticial lamellae. Mafic phases include greenish hornblende and light brown biotite, whereas accessory minerals include apatite, sphene, allanite and ilmenite. Zircon crystals are particularly rare and only observed as tiny inclusions in biotite. Chlorite is the main secondary mineral, resulting from biotite or hornblende alteration, whereas fine-grained epidote fibers are interpreted as the result of saussuritization. Point counting petrographic data indicates that the dominant rock type is monzogranite; however, granodiorites and tonalites represent subordinate members (Fig. 4) (see Fig. 5).

3. Analytical procedures

U-Pb zircon dating was obtained via Laser Ablation Inductively Coupled Plasma Mass Spectrometry (LA-ICP-MS) at the Geochronology Lab of the Universidade de Brasília. They include one sample from the São Caetano Complex and two form the São Pedro Stock with isotopic results presented in Tables 1–3. Selected samples were initially crushed and sieved, then the heavy minerals were separated using conventional gravimetric and magnetic methods. Zircon crystals were then handpicked using binocular microscope and embedded on epoxy resin. Scanning Electron Microscopy (SEM) was used in order to obtain cathodoluminescence and backscattering images to guide the isotopic analysis.

Data reduction was performed following Bühn et al. (2009) and Matteinni et al. (2009). Isotopic analyses were carried out on a Thermo Finnigan Neptune Multi-collector ICPMS equipped with a secondary electron multiplier-ion counter. Only coherent interval analyses were chosen to avoid mixed signal data. Normalization was performed with internal GJ standard zircon (608.5 ± 1.5 Ma; Jackson et al., 2004). The obtained ages were calculated using Isoplot version 4.1 (Ludwig, 2012), avoiding spots that present high concentrations of common Pb.

Sm-Nd analyses were performed on 22 samples, following the method described in Gióia and Pimentel (2000). Most of the Sm-Nd data presented in this work were already published (Santos et al., 2018), but in a research with a different focus and the overall isotopic results is presented on Table 4. Whole rock powders (~50 mg) were mixed with a ^{149}Sm-^{150}Nd spike solution and dissolved in Savillex capsules. The extraction of Sm and Nd from whole rock samples followed conventional cation exchange techniques using Teflon columns containing LN-Spec resin (HDEHP, diethylhexyl phosphoric acid

Table 1
Summary of LA-ICP-MS data of zircons from sample LS-162 (São Caetano Complex).

Grain Spot	Isotope ratios (%)										Ages (Ma)						
	$^{206}Pb/^{204}Pb$	f206 (%)	$^{207}Pb/^{206}Pb$	± (1σ)	$^{207}Pb/^{235}U$	± (1σ)	$^{206}Pb/^{238}U$	± (1σ)	Th/U	Rho	$^{207}Pb/^{206}Pb$	± (1σ)	$^{207}Pb/^{235}U$	± (1σ)	$^{206}Pb/^{238}U$	± (1σ)	Conc.(%)
004-Z01	58758	0.02	0.081	0.557	1.865	1.120	0.167	0.972	0.352	0.856	1165	11	1069	7	996	9	93
005-Z02	5543	0.29	0.109	0.523	4.432	0.878	0.294	0.705	0.550	0.771	1739	10	1718	7	1659	10	97
006-Z03	5427	0.31	0.077	0.845	1.705	1.214	0.160	0.871	0.461	0.694	1071	17	1011	8	957	8	95
008-Z05	15687	0.11	0.073	0.465	1.550	0.910	0.153	0.782	0.345	0.840	969	10	951	6	918	7	97
009-Z06	87951	0.02	0.130	0.571	6.120	1.080	0.341	0.917	0.008	0.834	2050	10	1993	9	1891	15	95
010-Z07	253075	0.01	0.122	0.428	5.493	0.924	0.327	0.819	0.422	0.871	1933	8	1900	8	1824	13	96
014-Z09	167536	0.01	0.073	0.571	1.602	1.203	0.159	1.059	0.264	0.871	960	12	971	8	950	9	98
015-Z10	62774	0.03	0.072	0.826	1.593	1.330	0.160	1.042	0.551	0.769	936	17	968	8	956	9	99
016-Z11	126036	0.01	0.071	0.916	1.538	1.223	0.157	0.811	0.354	0.633	895	19	946	8	942	7	100
017-Z12	70437	0.02	0.069	0.642	1.352	1.025	0.142	0.799	0.160	0.754	836	14	868	6	858	6	99
018-Z13	27430	0.06	0.073	1.512	1.674	2.167	0.166	1.552	0.423	0.709	958	32	999	14	991	14	99
020-Z15	375560	0.01	0.125	0.325	5.778	0.744	0.335	0.669	0.325	0.878	1978	6	1943	6	1864	11	96
023-Z16	59224	0.02	0.074	1.573	1.661	2.236	0.164	1.590	0.538	0.704	972	33	994	14	977	14	98
024-Z17	183340	0.01	0.073	0.513	1.551	1.010	0.154	0.870	0.053	0.846	961	11	951	6	922	7	97
025-Z18	138290	0.01	0.072	0.717	1.628	1.169	0.163	0.924	0.100	0.772	938	15	981	7	974	8	99
026-Z19	42365	0.04	0.074	0.998	1.491	1.453	0.147	1.057	0.717	0.711	972	21	927	9	884	9	95
027-Z20	41564	0.04	0.072	1.602	1.504	2.513	0.153	1.936	0.309	0.766	913	34	932	15	915	17	98
028-Z21	899	1.90	0.072	1.038	1.589	1.769	0.159	1.432	0.080	0.855	936	21	966	11	954	13	99
033-Z24	40195	0.04	0.077	2.321	1.659	2.837	0.156	1.631	0.329	0.568	1071	48	993	18	933	14	94
034-Z25	2034	0.84	0.071	1.090	1.540	1.429	0.156	0.923	0.443	0.658	912	22	947	9	936	8	99
035-Z26	358762	0.01	0.187	0.421	12.56	0.996	0.486	0.902	0.310	0.896	2672	7	2648	9	2555	19	96
036-Z27	77785	0.02	0.072	1.082	1.554	1.471	0.156	0.996	0.821	0.658	939	23	952	9	933	9	98
037-Z28	142356	0.01	0.113	0.664	4.780	1.052	0.306	0.816	0.475	0.751	1799	12	1781	9	1723	12	97
039-Z30	313031	0.01	0.072	0.413	1.577	0.934	0.159	0.838	0.409	0.884	926	9	961	6	951	7	99
045-Z33	116515	0.01	0.072	0.659	1.580	1.000	0.158	0.751	1.210	0.720	939	14	962	6	947	7	98
048-Z36	43481	0.04	0.074	1.158	1.691	2.071	0.165	1.717	0.411	0.825	987	24	1005	13	987	16	98
049-Z37	88337	0.02	0.072	1.206	1.566	1.743	0.158	1.259	0.866	0.711	923	25	957	11	946	11	99
050-Z38	4743	0.4	0.075	0.788	1.674	1.515	0.163	1.294	0.348	0.857	1002	16	999	10	971	12	97
055-Z41	28879	0.06	0.074	1.442	1.767	2.150	0.172	1.595	1.108	0.735	996	30	1034	14	1024	15	99
056-Z42	114216	0.01	0.073	0.646	1.674	1.104	0.166	0.894	0.373	0.792	959	14	999	7	990	8	99
057-Z43	54080	0.03	0.072	1.079	1.588	1.464	0.159	0.990	0.682	0.657	941	23	966	9	951	9	98
058-Z44	132809	0.01	0.074	0.436	1.696	0.910	0.165	0.799	0.490	0.861	995	9	1007	6	986	7	98
059-Z45	52125	0.03	0.075	1.761	1.778	2.227	0.171	1.364	0.616	0.602	1024	37	1037	14	1017	13	98
063-Z48	3402	0.5	0.074	0.640	1.633	1.171	0.160	0.980	0.086	0.838	984	13	983	7	956	9	97
064-Z49	97102	0.02	0.072	0.888	1.541	1.316	0.156	0.972	0.867	0.720	924	19	947	8	932	8	98
066-Z51	83208	0.02	0.072	0.647	1.503	1.135	0.151	0.933	0.381	0.806	929	14	931	7	908	8	97
068-Z53	70506	0.02	0.073	0.073	1.547	1.320	1.146	0.860	0.497	0.860	944	14	949	8	927	10	98
074-Z57	32447	0.05	0.073	0.073	1.504	1.177	0.929	0.771	0.526	0.771	945	15	932	7	902	8	97
075-Z50	96402	0.02	0.107	0.107	4.211	1.841	1.576	0.852	0.413	0.852	1695	18	1676	15	1620	23	97
076-Z59	15164	0.11	0.079	0.079	1.847	1.333	0.780	0.551	0.390	0.551	1127	22	1062	9	1004	7	95
077-Z60	1931	0.88	0.076	0.076	1.732	1.373	0.896	0.663	0.458	0.663	1050	21	1020	9	981	8	96
078-Z61	75498	0.02	0.093	0.093	3.507	1.404	1.086	0.760	0.140	0.760	1441	17	1529	11	1553	15	102
014-Z9	77030	0.02	0.074	0.864	1.620	1.365	1.057	0.760	0.527	0.760	975	18	978	9	954	9	98
035-Z26	129686	0.01	0.071	1.212	1.263	1.846	1.392	0.746	0.379	0.746	910	26	829	10	888	10	94
041-Z30	40229	0.4	0.074	0.802	1.757	1.249	0.958	0.749	0.396	0.749	982	17	1030	8	1025	9	100
054-Z42	2923	0.58	0.068	0.784	1.420	1.905	1.737	0.920	0.248	0.920	812	16	897	11	908	15	101
074-Z59	290607	0.05	0.112	0.484	4.795	1.413	1.327	0.937	0.895	0.937	1778	9	1784	12	1745	20	98

Table 2
Summary of LA-ICP-MS data of zircons from sample LS-89 (São Pedro Stock).

Grain Spot	Isotope ratios (%)										Age (Ma)						
	$^{206}Pb/^{204}Pb$	f206 (%)	$^{207}Pb/^{206}Pb$	± (1σ)	$^{207}Pb/^{235}U$	± (1σ)	$^{206}Pb/^{238}U$	± (1σ)	Th/U	Rho	$^{207}Pb/^{206}Pb$	± (2σ)	$^{207}Pb/^{235}U$	± (2σ)	$^{206}Pb/^{238}U$	± (1σ)	Conc. (%)
017-ZR45	2802	0.073	0.06141	1.03	0.849	1.71	0.1003	1.31	0.130	0.77	654	44	624	16	616	15	95
052-ZR24	4749	0.038	0.06021	1.26	0.838	1.68	0.1010	1.06	0.252	0.63	611	54	618	16	620	12	99
048-ZR22	82344	0.003	0.06217	0.67	0.852	1.17	0.0993	0.89	0.395	0.76	680	28	626	11	611	10	90
027-ZR12	170283	0.009	0.06044	0.53	0.823	1.25	0.0988	1.07	0.282	0.85	619	23	610	11	607	12	99
016-ZR8N	49850	0.002	0.06120	0.92	0.835	1.56	0.0990	1.20	0.464	0.77	646	39	617	14	608	14	95

Table 3
Summary of LA-ICP-MS data of zircons from sample LS-35B (São Pedro Stock).

Grain Spot	Isotope ratios (%)										Ages (Ma)						
	$^{206}Pb/^{204}Pb$	f206 (%)	$^{207}Pb/^{206}Pb$	± (1σ)	$^{207}Pb/^{235}U$	± (1σ)	$^{206}Pb/^{238}U$	± (1σ)	Th/U	Rho	$^{207}Pb/^{206}Pb$	± (1σ)	$^{207}Pb/^{235}U$	± (1σ)	$^{206}Pb/^{238}U$	± (1σ)	Conc. (%)
008-Z005	3129	0.057	0.061	1.24	0.825	1.81	0.098	1.32	0.330	0.71	584	28	611	8	602	8	98
009-Z006	2311	0.077	0.062	1.86	0.800	2.58	0.093	1.79	0.588	0.68	626	41	597	12	573	10	96
010-Z007	26918	0.064	0.077	1.00	1.621	1.69	0.152	1.37	0.472	0.80	1077	21	978	11	911	12	93
015-Z010	19464	0.083	0.098	1.53	3.670	2.34	0.271	1.77	0.728	0.75	1539	30	1565	19	1544	24	99
017-Z012	50263	0.034	0.079	1.25	1.684	3.35	0.154	3.10	0.409	0.92	1123	26	1002	21	923	27	92
018-Z013	705	2.546	0.064	3.75	0.655	4.94	0.074	3.21	0.363	0.74	679	78	512	20	462	14	90
019-Z014	1281	1.385	0.059	2.04	0.787	2.55	0.097	1.52	0.580	0.65	492	44	590	11	599	9	102
023-Z015	27448	0.062	0.072	1.17	1.621	1.70	0.163	1.22	0.175	0.70	937	25	979	11	971	11	99
025-Z17	37806	0.046	0.069	2.32	1.272	3.39	0.134	2.47	0.898	0.72	838	50	833	19	809	19	97
026-Z18	29713	0.059	0.063	0.91	0.921	1.62	0.106	1.34	0.301	0.82	637	20	663	8	652	8	98
029-Z21	1615	0.106	0.075	1.65	1.728	2.38	0.168	1.72	0.419	0.71	1005	34	1019	15	999	16	98
032-Z23	7542	0.023	0.073	1.07	1.607	1.90	0.160	1.57	0.448	0.82	956	23	973	12	955	14	98
036-Z27	7647	0.232	0.068	2.01	0.904	2.81	0.097	1.96	0.436	0.69	800	44	654	14	596	11	91
038-Z29	97505	0.002	0.073	1.29	1.457	1.68	0.144	1.07	0.171	0.62	968	27	913	10	867	9	95

Table 4
Summary of Nd isotope data for the metaplutonic rocks of São Caetano Complex (S.C.C.) and São Pedro Stock (S.P.S.).

Sample	Unit	Sm (ppm)	Nd (ppm)	$^{143}Nd/^{144}Nd$ (± 2SE)	εNd (0)	εNd (0.86)	U-Pb age (Ga)	T_{DM} (Ga)
FL84A	S.C.C.	3.66	13.75	0.512565 (± 15)	−1.42	2.52	0.858	1.36
FL36	S.C.C.	6.69	35.60	0.512134 (± 24)	−9.84	−0.69	0.858	1.37
FL162	S.C.C.	6.06	32.81	0.512091 (± 12)	−10.66	−1.31	0.858	1.41
FL97	S.C.C.	2.15	12.12	0.512009 (± 26)	−12.27	−2.45	0.858	1.47
FL96	S.C.C.	2.15	12.12	0.512009 (± 26)	−12.27	−3.50	0.858	1.61
FL166	S.C.C.	5.96	28.75	0.512092 (± 15)	−10.65	−2.80	0.858	1.62
FL48	S.C.C.	2.34	11.15	0.512089 (± 21)	−10.72	−3.01	0.858	1.66
FL127G	S.C.C.	4.24	35.33	0.511473 (± 17)	−22.72	−9.09	0.858	1.68
FL167	S.C.C.	8.04	43.97	0.511871 (± 14)	−14.96	−5.50	0.858	1.72
FL160	S.C.C.	7.44	39.90	0.511888 (± 15)	−14.63	−5.40	0.858	1.73
FL49	S.C.C.	3.87	18.50	0.512045 (± 38)	−11.56	−3.84	0.858	1.73
FL164	S.C.C.	5.81	28.82	0.5119800 (± 07)	−12.83	−4.62	0.858	1.75
FL163	S.C.C.	6.45	32.02	0.511974 (± 13)	−12.95	−4.71	0.858	1.76
FL168	S.C.C.	8.43	45.32	0.511843 (± 17)	−15.5	−6.25	0.858	1.79
FL85	S.C.C.	3.49	18.50	0.511844 (± 15)	−15.48	−6.40	0.858	1.82
FL84B	S.C.C.	4.37	16.16	0.512424 (± 21)	−4.17	−0.51	0.858	1.85
FL38	S.C.C.	3.53	16.52	0.511947 (± 19)	−13.48	−6.04	0.858	1.96
FL35B	S.P.S.	3.72	20.13	0.511937 (± 07)	−13.67	−7.21	0.596	1.64
FL92	S.P.S.	5.74	40.33	0.511558 (± 12)	−21.07	−12.66	0.596	1.76
FL78A	S.P.S.	3.87	29.50	0.511470 (± 24)	−22.78	−13.86	0.596	1.77
FL78B	S.P.S.	0.35	2.19	0.511657 (± 23)	−19.14	−11.45	0.596	1.78
FL80A	S.P.S.	4.10	27.13	0.511554 (± 02)	−21.15	−13.13	0.596	1.84
FL89	S.P.S.	2.91	20.15	0.511502 (± 08)	−22.16	−13.85	0.596	1.85

Table 5
Major (wt. %) and trace element (ppm) concentrations of the São Caetano Complex.

Sample	FL37	FL97	FL159	FL160	FL161	FL162	FL164	FL167	FL168
Major elements (wt.%)									
SiO_2	69.7	65.5	66.0	63.3	70.0	70.2	62.8	62.4	60.9
TiO_2	0.60	0.79	0.75	0.74	0.58	0.58	0.74	0.78	0.81
Al_2O_3	14.0	15.0	14.9	15.8	13.8	13.9	15.7	15.7	16.3
Fe_2O_3(total)	3.77	6.14	6.29	6.29	3.63	3.67	6.35	6.21	6.28
MnO	0.06	0.07	0.09	0.09	0.06	0.06	0.09	0.07	0.08
MgO	1.40	1.35	1.28	1.21	1.35	1.37	1.22	1.28	1.36
CaO	1.50	1.59	2.33	2.34	1.49	1.48	2.34	1.60	1.64
Na_2O	1.96	2.43	2.02	2.05	1.95	1.95	2.05	1.92	2.38
K_2O	2.58	4.10	3.83	3.53	2.49	2.53	3.55	3.84	4.19
P_2O_5	0.05	0.05	0.04	0.06	0.05	0.04	0.06	0.05	0.05
LOI	2.75	4.22	4.28	4.34	2.70	2.76	4.17	4.27	4.25
Total	98.37	101.2	101.8	99.75	98.10	98.54	99.07	98.12	98.24
Trace elements (ppm)									
V	2.45	1.31	1.29	1.32	2.51	2.76	1.39	1.35	1.34
Cr	70.0	80.0	70.0	70.0	60.0	70.0	70.0	70.0	70.0
Ga	19.6	22.1	22.9	23.4	21.7	19.6	24.5	23.4	23.1
Rb	112	151	140.5	141	106	109.5	145	150	147.5
Sn	3.00	3.00	3.00	3.00	2.00	3.00	4.00	3.00	3.00
Sr	193.5	265	382	375	185	194	392	262	255
W	168	222	200	195	161	165	210	222	214
Zr	229	210	186	179	223	263	209	186	195
Nb	14.0	11.5	11.0	11.0	13.0	13.7	11.7	11.8	11.6
Cs	5.03	1.50	1.3	1.39	4.64	4.86	1.44	1.57	1.59
Ba	811	1055	991	986	828	804	1020	1060	1015
La	52.5	46.1	41.6	40.0	47.8	55.6	42.1	44.2	43.4
Ce	109.5	92.6	84.9	82.9	112	116	87.9	88.7	87.0
Pr	12.3	10.7	9.72	9.78	11.3	13.4	9.89	10.2	10.5
Nd	44.0	40.4	36.3	36.4	43.9	47.0	35.9	40.3	38.9
Sm	8.16	7.21	6.58	6.05	8.14	8.11	6.58	7.15	6.12
Eu	1.65	1.89	1.92	1.96	1.60	1.82	1.94	1.85	1.73
Gd	6.69	6.06	5.90	5.61	6.93	7.12	6.41	5.47	6.17
Tb	0.96	0.82	0.81	0.81	1.00	1.09	0.89	0.85	0.82
Dy	5.58	4.80	5.07	4.91	5.35	5.78	5.37	4.33	4.38
Ho	0.98	0.86	0.97	1.03	1.05	1.18	1.08	0.85	0.78
Er	2.90	2.38	2.77	2.88	3.00	3.34	3.34	2.45	2.15
Tm	0.44	0.40	0.43	0.50	0.45	0.50	0.44	0.37	0.32
Yb	3.18	2.44	3.00	2.90	2.58	3.23	3.07	2.38	2.47
Lu	0.44	0.36	0.47	0.42	0.45	0.49	0.52	0.36	0.33
Y	29.5	23.9	26.7	27.1	27.0	33.1	28.1	23.2	22.0
Hf	6.50	5.60	5.00	5.10	6.10	7.00	5.80	5.30	5.20
Ta	1.00	0.70	0.70	0.70	1.40	1.00	1.00	0.70	0.80
Th	15.2	10.9	9.10	9.20	14.3	16.5	9.74	10.3	9.86
U	2.45	1.31	1.29	1.32	2.51	2.76	1.39	1.35	1.34

Table 6
Major (wt. %) and trace element (ppm) concentrations of the São Pedro Stock.

Sample	FL28	FL30	FL81	FL83	FL84	FL90	FL91	FL92	FL93	FL94
Major elements (wt.%)										
SiO_2	69.3	69.2	71.2	69	70.6	71.6	70.4	69.5	70.5	70.5
TiO_2	0.17	0.18	0.17	0.18	0.2	0.17	0.21	0.18	0.16	0.19
Al_2O_3	16	16.4	15.3	16.3	16.7	16.4	16.4	16.4	15.8	16.5
Fe_2O_3(total)	0.94	0.93	1.03	0.99	1.11	0.91	1.1	0.98	0.9	1.01
MnO	N.d	N.d	0.01	0.01	0.01	0.01	0.01	N.d	N.d	0.01
MgO	0.19	0.2	0.23	0.2	0.22	0.21	0.24	0.19	0.18	0.2
CaO	1.07	0.98	1.09	1.08	1.22	1.23	0.93	0.92	1.01	1.01
Na_2O	5.85	5.84	5.2	5.5	5.27	5.47	5.29	5.6	5.44	5.35
K_2O	3.69	3.91	3.76	4.37	4.33	3.86	4.18	3.94	3.79	3.88
P_2O_5	0.06	0.08	0.09	0.08	0.13	0.08	0.15	0.07	0.07	0.08
LOI	2.2	1.13	1.97	1.36	0.46	0.49	0.48	0.75	0.95	0.71
Total	98.53	98.85	100.05	99.07	100.25	100.43	99.39	98.53	98.80	99.44
Trace elements (ppm)										
V	N.d	N.d	N.d	N.d	9	8	12	N.d	N.d	9
Cr	N.d	N.d	N.d	N.d	20	20	20	N.d	N.d	30
Co	107	116	482	169	N.d	N.d	N.d	141	55	N.d
Mo	N.d	0.1	0.1	N.d	N.d	N.d	N.d	0.1	N.d	N.d
Ni	0.6	0.5	1.8	0.7	N.d	N.d	N.d	1	0.4	N.d
Cu	0.8	0.6	1	1	N.d	N.d	N.d	1.8	1	N.d
Zn	96	75	72	66	N.d	N.d	N.d	111	95	N.d
Ga	23.5	22	24	26.8	28.6	28	27.4	23.5	23.4	28
Rb	59.5	65.9	73.2	78.3	82.6	74.2	83.8	70.6	68.8	77.9
Sn	1	1	N.d	1	1	2	2	1	1	2
Sr	2620.9	2736.1	2366.1	2347.8	2440.1	2320.1	2790.1	2492.1	2463.7	2600.1
W	987	1347.4	3112.9	1730.6	787	1390	969	1522.2	741.2	706
Zr	133.7	155.1	126.1	140.7	166.1	151.1	161.1	147.2	138.1	164.1
Nb	10.5	11.6	9.3	12.2	15.2	11.5	12.4	11.9	10.8	15.1
Cs	0.9	1.3	1.6	0.9	0.97	1.64	2.08	1.9	1.5	1.96
Ba	4642	4969	3957	4148	4120	3860	5150	4339	4226	4320
La	34.5	4.8	5.7	9.5	10.2	47.5	40.6	35.5	18.1	66.4
Ce	56.1	17.3	35.3	27.2	28.9	74.8	66.9	66.8	30.3	115
Pr	6.54	1.5	1.52	2.2	2.42	8.45	7.23	7.22	3.49	12.9
Nd	24.7	6.7	5.8	8.2	9.8	28.4	25.8	23.9	12.9	41.0
Sm	3.82	1.69	1.39	1.73	2.2	4.26	3.76	3.76	1.98	5.23
Eu	1.15	0.55	0.46	0.59	0.55	0.97	1.01	0.95	0.64	1.47
Gd	2.28	1.09	0.9	0.9	1.01	1.94	1.61	1.72	1.11	2.35
Tb	0.16	0.09	0.06	0.07	0.11	0.18	0.16	0.14	0.09	0.19
Dy	0.51	0.2	0.21	0.18	0.36	0.67	0.51	0.42	0.27	0.71
Ho	0.05	0.03	N.d	0.04	0.04	0.1	0.08	0.04	N.d	0.11
Er	0.11	0.05	0.11	0.06	0.13	0.16	0.1	0.1	0.1	0.24
Tm	0.02	N.d	0.02	0.01	N.d	0.02	N.d	0.02	0.01	0.02
Yb	0.09	0.08	0.09	0.09	0.11	0.09	0.13	0.11	0.06	0.16
Lu	N.d	0.01	N.d	0.01	N.d	N.d	N.d	0.01	0.02	0.01
Y	1.7	0.7	1.0	1.1	1.2	2.5	1.9	1.4	1.1	2.8
Hf	3.6	4.5	4.3	4.7	5.2	4.7	5.3	4.6	4.2	5.1
Ta	0.8	1	1.2	1.1	1	1.1	0.9	1.2	0.8	1.1
Pb	8.7	8.8	9.9	9.4	N.d	N.d	N.d	12.7	7.8	N.d
Th	8.9	9.8	7.2	8.4	9.1	9.25	13.75	9.7	8.2	11.1
U	1.7	1.7	2.3	2.5	2.35	1.85	2.51	2.5	1.6	2.39

supported on PTFE powder). The Sm and Nd samples were loaded on Re evaporation double-filament assemblies. The isotopic measurements were performed using a Triton Plus Thermoscientific multicollector mass spectrometer in the static mode. The uncertainties in the Sm/Nd and $^{143}Nd/^{144}Nd$ ratios are better than ± 0.2% (2σ) and ± 0.0064% (1σ), respectively, based on repeated analyses using the BHVO-2 international rock standard. The $^{143}Nd/^{144}Nd$ ratios were normalized to a $^{146}Nd/^{144}Nd$ ratio of 0.7219, and a decay constant of 6.54×10^{-12}/year was used (Lugmair et al., 1978). The T_{DM} model ages were calculated using the DePaolo (1981) model.

Representative fresh rock samples were carefully selected for whole-rock geochemical analysis and the obtained results are presented in Tables 5 and 6. A total of 21 samples (9 from the São Caetano Complex and 12 from the São Pedro Stock) were analyzed via Induced Coupled Plasma Mass Spectrometry (ICP-MS) and inductively coupled plasma atomic emission spectroscopy (ICP-AES) at the Acme (Canada) and ALS (Peru) laboratories. Major and trace elements were analyzed by ICP-AES with detection limit of 0.01% and ICP-MS with detection limit between 0.01 and 0.5 ppm after fusion using Li meta- and tetraborate and digestion with nitric acid. The percentage of Loss on Ignition was determined by the difference in sample weight before and after heating at 1000 °C for 1 h. Geochemical diagrams were generated using Igpet 06, GCDkit and Petrograph softwares as well as Excel sheets.

4. Results

4.1. U-Pb geochronology

4.1.1. Sample FL-162 (São Caetano Complex)

Sample FL-162 is a biotite-muscovite schist from the São Caetano Complex (geographic coordinates 38°33′41″W and 08°21′09″S). Zircon crystals from this rock range in size from 60 to 140 μm with 1:1 and 1:5 axial ratios. Most grains display a prismatic subhedric crystalline habit, including sub-rounded multifaceted, pyramidal finely zoned crystals and ovoid shapes. Anhedral grains are also present as a minor component and xenocryst cores are absent. Growth oscillatory zoning is typical for prismatic grains and Th/U ratios are always higher than 0.1, supporting a magmatic-derived source. A cluster of 50 grains points out

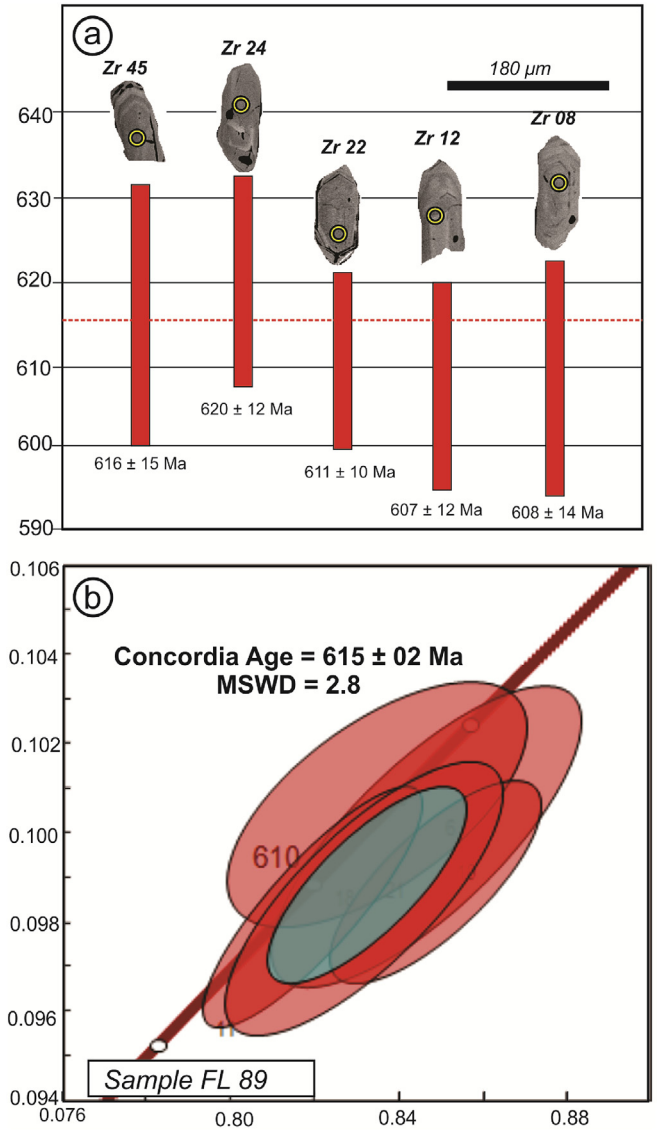

Fig. 6. Sample FL-89 (hornblende-biotite tonalite): a) Cathodoluminescence images of the analyzed zircon crystals and spot locations; b) Concordia diagram showing the interpreted crystallization age.

to a major peak at around 1000 Ma with the youngest grain dated at *ca.* 858 Ma (all ages discussed are $^{206}Pb/^{238}U$ dates; Stern, 1997). Seven grains yield discordant Paleoproterozoic ages (1.7-1.5 Ga) and there is a single Neoarchean age (*ca.* 2.6 Ga). Three zircon grains have Th/U smaller than or equal to 0.08 (z17, z21, z48) with apparent ages at 922, 954, and 956 Ma.

4.1.2. Sample FL-89 (São Pedro Stock)

Sample FL-89 is a hornblende-biotite monzogranite. It was collected close to the São Pedro strike-slip shear zone (geographic coordinates 38°23′29″W and 08°28′06″S), but does not display any evidence of deformation. Surprisingly, more than 100 kg of sample were crushed and after several attempts, 32 grains were collected. The vast majority of them are metamict, strongly fractured, or substantially discordant. The remaining five grains are morphologically similar, with sizes around 80 µm and axial shapes between 1:1 and 1:2. They display discrete regular growth oscillatory zoning, prismatic pyramidal shapes and tiny rim overgrowths, lacking inherited cores. The analyzed grains are mostly concordant and present Th/U ratios varying from 0.13 to 0.46, suggesting an igneous origin. These grains yield a Concordia age of 615 ± 2 Ma (MSWD = 2.8, Fig. 6) (see Fig. 7).

4.1.3. Sample FL-35B (São Pedro Stock)

Sample FL-35B represents a medium-grained, pinkish hornblende-bearing granodiorite collected at the east termination of the São Pedro stock (geographic coordinates 38°30′11″W and 08°32′19″S). Similar to sample FL-89, this rock is zircon poor; nevertheless, the studied grains are idiomorphic and exhibit bypiramidal to prysmatic well-developed shapes. They have dimensions greater than 100 µm and axial ratios between 1:1 and 1:3. A total of fourteen grains was analyzed; however, most show high discordance and only two distinct groups were used to calculate ages. A cluster of four concordant zircon crystals with oscillatory zoning and Th/U ratios > 0.1 yields a Concordia age of 981 ± 21 Ma (MSWD = 6.7), interpreted as inherited grains of Tonian crust, whereas the other cluster yields an average age of 596 ± 22 Ma ($^{206}Pb/^{238}U$, MSWD = 3.9), which is interpreted as the crystallization age of the rock.

4.2. Sm-Nd isotopes

Metasedimentary rocks of the São Caetano Complex are characterized by mid-Meso- to Paleoproterozoic Nd depleted mantle T_{DM} model-ages, ranging between 1.36 and 1.96 Ga. The $\varepsilon Nd_{(0.858)}$ values calculated using the maximum deposition age, range from positive to negative (+3.03 to −5.24) indicating juvenile and reworked detrital sources. The samples of the São Pedro Suite also present Meso-to Paleoproterozoic T_{DM} model-ages, ranging from 1.64 to 1.85 Ga, and show strongly negative $\varepsilon Nd_{(t)}$ values ranging between −7.21 and −13.85, calculated for the 596 Ma crystallization age.

4.3. Whole-rock geochemistry

4.3.1. São Caetano Complex

Whole-rock geochemistry was conducted on biotite-muscovite schists, which are the most representative rock type of this unit in the area. The analyzed rocks show moderate to relatively high concentrations of SiO_2 (60.9–70.2 wt%), high Al_2O_3 (13.8–16.3 wt%), and low K_2O and Na_2O values (2.53–4.19 wt% and 1.2–1.40 wt%, respectively). The distribution of trace elements on normalized spiderdiagrams show negative anomalies of U, Nb and Sr (Fig. 9a). The rare earth element (REE) patterns normalized to the chondrite values of Nakamura (1974), show moderate slope, being characterized by mild light REE enrichment over heavy REE [(La/Yb) = 9.12–12.60] with negative Eu anomalies [(Eu/Eu*) = 0.65–1.03]. Also, the general patterns of the REE are similar to those of the North American Shale Composite (NASC) and the Upper Continental Crust (UCC) (Fig. 9b). On the ternary diagram of molar proportions of $A(Al_2O_3)$ - $Cn(CaO + Na_2O)$ - $K(K_2O)$ of Nesbitt and Young (1982), the samples are richer in Al_2O_3 as compared to the other major elements, whereas in comparison to the Chemical Index of Alteration (CIA), they are characterized by relatively intense weathering degree (65–75, Fedo et al., 1995) in the source area (Fig. 10a) (see Fig. 8).

In the $Log(K_2O/Na_2O)$ vs. SiO_2/Al_2O_3 discriminant diagram for sedimentary/metasedimentary rocks, the samples plot in the ACM field, which is indicative of detritial material derived from active continental margins (Roser and Korsch, 1988, Fig. 10b). A similar inferred origin was obtained in the $log(K_2O/Na_2O)$ vs. SiO_2 diagram of Maynard et al. (1982; Fig. 10c). In the Hf vs. La/Th diagram of Floyd and Leveridge (1987), the analyzed samples plot in the field of detrital material derived from intermediate/acid magmatic arc sources (Fig. 10d).

4.3.2. São Pedro Stock

In terms of overall geochemical parameters, the samples are homogeneous for most major and trace elements. Fig. 11 shows the chemical classification proposed by De La Roche et al. (1980) for the granitoids, showing that they correspond to granites with minor

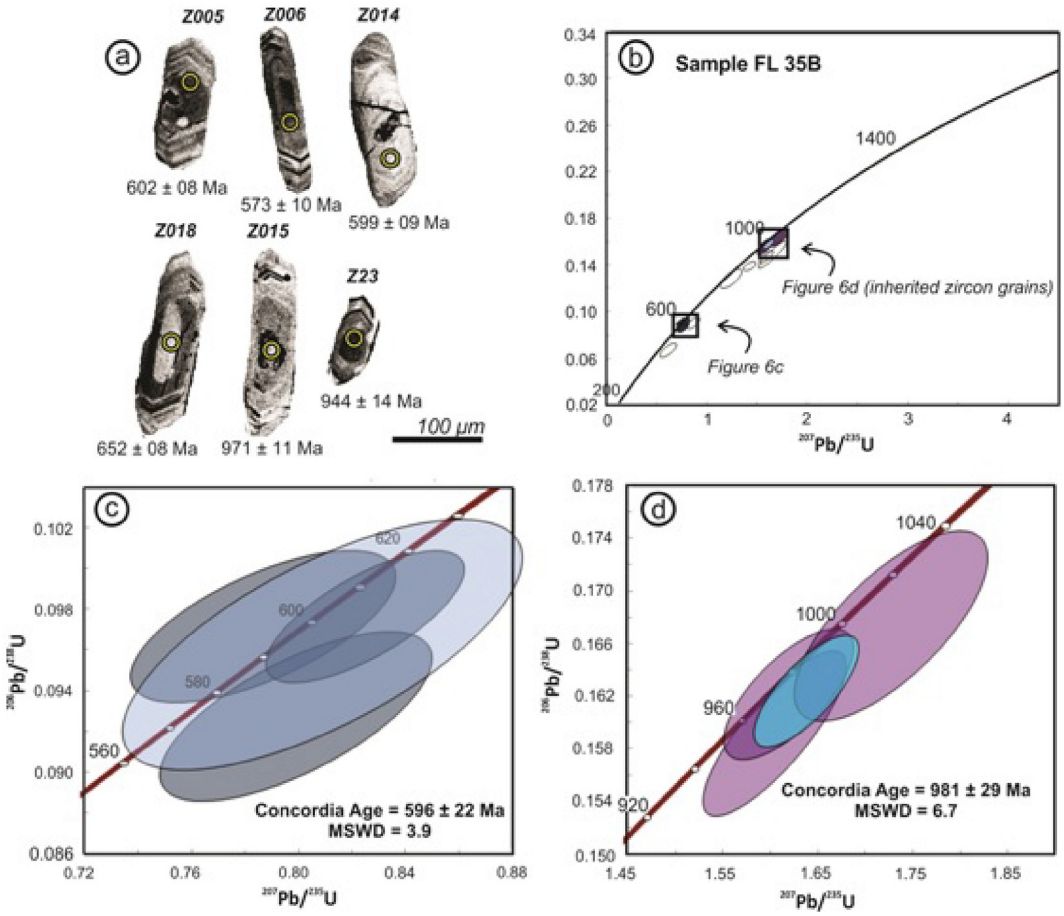

Fig. 7. Sample FL-35B (hornblende-bearing granodiorite): a) Cathodoluminescence images of the analyzed zircon crystals and spot locations; b) Concordia diagram with zircon grains plotted, c) and d) concordant zircon crystals defining the proposed crystallization and inherited ages, respectively.

presence of tonalites, which is in accordance with the petrographic study. They have SiO_2 values around 70 wt%, moderate contents on Na_2O, ranging from 3.85 to 5.8 wt% and intermediate K_2O values, ranging from 3.8 to 4.6 wt%. These parameters suggest that the studied rocks share similarities with calc-alkaline and slightly alkaline granites (Fig. 12a), representing magmas of the high K-calc-alkaline series (Fig. 12b). On the SiO_2 vs. FeOt/(FeOt + MgO) diagram from Frost et al. (2001), the samples share chemical similarities with Cordilleran type-granites (FeOt and MgO values ranging from 0.90 to 1.03 and 0.1 to 0.7 wt%, respectively), plotting in the transition between the magnesian and ferroan series (Fig. 12c). Also, in the A/NK vs. A/CNK diagram, modified by Maniar and Piccoli (1989), the studied samples are slightly peraluminous, but show Al_2O3, Na_2O, K_2O and CaO values compatible with I-type granites (Fig. 12d). Other analyzed major element contents are low, including TiO_2 (0.1–0.4 wt%) and P_2O_5 (0.05–0.16 wt%).

Trace element distribution on spiderdiagrams were normalized to the values of Thompson (1982), and are characterized by high contents of large ion lithophile elements (LILE), including Rb, Ba and K and lower concentrations of high field strength elements (HFSE). In addition, the samples are characterized by moderate negative anomalies on Nb, Ta, Nd, Sm and Ti as well as positive peaks on Ba, K, Sr and Zr (Fig. 13a). The REE pattern for the studied samples, normalized to the chondrite values of Nakamura (1974) is also relatively homogeneous. The sum of REE values ranges from 34.09 to 246.35 and the overall distribution is characterized by moderate fractionation of light compared to heavy REE (Fig. 13b; $(La/Tb)_N$ ranging from 40.0 to 351.8) and lacks any evidence of significant negative Eu anomalies (Eu/Eu* = 1.04–1.45).

In the TiO_2 vs. Zr diagram of Hine et al. (1978), the granites plot in the I-type granitic field (Fig. 14a) and are chemically similar to fractionated granite magmas in the Na_2O/K_2O + CaO versus Zr + Nb + Cd + Y diagram (Fig. 14b) of Whalen et al. (1987). On tectonic discrimination diagrams, the samples show geochemical signatures compatible to magmas generated at active continental margins (Fig 14c; Schandl and Gorton, 2002), plotting within the volcanic arc granite (VAG) field (Fig. 14d, e) on the diagrams of Pearce et al. (1984) as well as evolving to late orogenic granites on the diagram of Batchelor and Bowden (1985; Fig. 14f).

5. Discussion

5.1. Age, provenance and tectonic setting of the São Caetano Complex

The São Caetano Complex was originally defined as a series of mica schists, metagraywackes, metapelites, metapsamites, metavolcanic and metavolcanoclastic rocks with minor marble and calc-silicate members (Kozuch, 2003; Santos et al., 2010). In the study area, this unit is strongly affected by thrust and strike-slip tectonics and biotite-muscovite schists predominate. Metavolcanic and metavolcanoclastic rocks are restricted to isolated occurrences. Detrital U-Pb zircon data from a biotite-muscovite schist yield early Neoproterozoic maximum depositional ages (1.0-0.9 Ga), with minor contributions of Archean and Paleoproterozoic sources (2.5-1.7 Ga). At least, three detrital zircon crystals aged at around 1025 Ma fits with the age of the Serrote das Pedras Pretas Suite (Lages and Dantas, 2016). A single Neoarchean grain could have been supplied from the Riacho das Lajes Suite, in which case the Alto Pajeú Terrane have already docked in the Alto

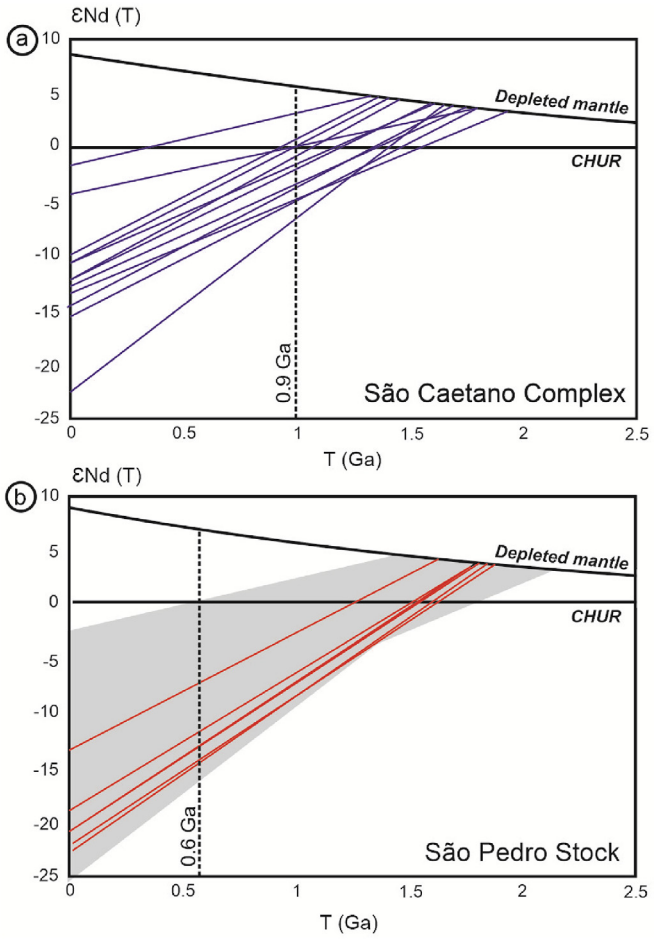

Fig. 8. Nd isotopic composition for the studied rocks of the a) São Caetano Complex and b) São Pedro Stock. The grey field in fig. b illustrates the range of Nd isotope epsilon Nd shown in fig. a.

Moxotó during the deposition of the São Caetano Complex as suggested by Santos et al. (2017b, 2018). Thus, we interpret the ca. 1000-920 Ma CVB metaplutonic sequences as the main source of detritus, through the erosion of the arc edifice. However, a concordant zircon at 858 Ma post-dates the period of main magmatism in the CVB (ca. 1000-960 Ma), but is roughly coeval with anorogenic units further south in the Riacho do Pontal Belt, such as the Brejo Seco mafic-ultramafic complex (ca. 900 Ma; Salgado et al., 2016) and the Paulistana rift volcanosedimentary sequence (ca. 882 Ma; Caxito et al., 2016) and represents the maximum deposition age of the São Caetano Complex in the region. Well documented detrital zircon data and associated bimodal magmatism in other supracrustal sequences of the province are quite younger (ca. 750 Ma; Arthaud et al., 2015).

The obtained T_{DM} model ages in this study are slightly older than the available data of this sequence in the literature (*i.e.* 1.6-1.2 Ga; Van Schmus et al., 1995; Kozuch, 2003) and coupled with ε_{Nd} values, support derivation from reworked Meso-to late Paleoproterozoic crust. General whole-rock geochemical data, including trace-element distribution and tectonic discriminant diagrams are indicative of derivation from continental magmatic arc-related rocks, whose chemical composition varies from intermediate to acid (*i.e.* andesitic-rhyolitic). REE elements distribution coincides with values of NASC and UCC, supporting a strong continental component in the source region.

Stenian to Tonian units of the Borborema Province are assumed to be generated during the Cariris Velhos tectonic event, whose nature is still under discussion. Some authors argue that rocks of this age were mainly generated in a continental magmatic arc-back-arc system (Kozuch, 2003; Santos et al., 2010; Caxito et al., 2014a). This interpretation is based on the recognition of several calc-alkaline and peraluminous volcanic and granitic suites with arc-related and syn-collisional geochemical signatures. Recent investigations of high-pressure metamorphosed mafic-ultramafic rocks of *ca.* 1024 Ma, interpreted as intra-oceanic sequences (*i.e.* Serrote das Pedras Pretas Suite, Lages and Dantas, 2016), as well as magnetotelluric signatures revealing a fossil subduction zone (Padilha et al., 2016), also favors an orogenic origin. In addition, a close temporal relationship between the Cariris Velhos units within the Rodinia supercontinent assembly has also been proposed (Fuck et al., 2008; Santos et al., 2010), being developed prior its major break-up stage at 750 Ma (Li et al., 2008).

Conversely, geochronological and isotopic data of supracrustal rocks of the CVB have been interpreted as the record of two early rifting episodes at *ca.*1091-920 Ma and 806 Ma (Guimarães et al., 2012). An-orogenic geochemical signature of orthogneisses and metagranites throughout the province are indicative of continental extension (Guimarães et al., 2015) as well as the fact that collisional metamorphism of Cariris Velhos age was not yet described (Neves, 2003, 2015). Regarding the last point, it should be noted that in this study, we found three detrital zircon grains with low Th/U ratios (0.086, 0.080 and 0.053) with ages between 956 and 922 Ma. Lages and Dantas (2016) described one $^{238}U/^{206}Pb$ age from a zircon core of 967 ± 9 Ma suggesting concomitant metamorphic processes after crystallization of the SPP Suite.

The overall geochemical and isotope signature of the studied rocks are compatible with sedimentary sequences derived from exhumed continental magmatic arcs (Bathia and Crook, 1986). Thus, we suggest that the precursor sedimentary pile of the São Caetano Complex strongly derived from a volcano-plutonic accretionary system, also presenting minor contributions of foreland material. Our statement is mostly based on the i) geochemical "arc-derived signature" of the studied samples, ii) temporal relationship of detritus and their sources as well as the Nd signature of calc-alkaline Cariris Velhos granites/orthogneisses (Kozuch, 2003) and iii) spatial relationship between the São Caetano Complex and the mafic-ultramafic pile of the Serrote das Pedras Pretas cumulatic-ophiolitic sequence. Back-arc settings might evolve to post-collisional lithospheric extension, which is triggered by hinge roll-back, post-dating terrane accretion (Sdrolias and Muller, 2006). This process might involve large degrees of partial melting of the continental crust and subsequent orogenic collapse, producing a number of magma types and incorporation of detritus from variable crust segments, including the magmatic arc, obducted sequences and the host continental margin (Keskin, 2003; Madsen et al., 2006).

A syn-to post-orogenic continental spreading might explain the "anorogenic" signature of the Cariris Velhos units described within the Borborema Province by Guimarães et al. (2015). In fact, a viable explanation for the occurrence of both convergent and extensional signatures in the plutonic and volcanic units of the CVB is the presence of later back-arc domains or within-plate sites. In the proposed scenario, the Alto Moxotó Terrane could have acted as a foreland basement during lithospheric collision which is generally coeval to break-off episodes of the subducted plate (Fig. 15a). Subsequent crustal extension documented in supracrustal rocks within the CVB that are aged around ca. 806 Ma (Guimarães et al., 2012) and 858 Ma herein, might represent a continental stretching phase coeval to orogenic collapse (Fig. 15b) such as proposed for the Riacho do Pontal Belt in the Southern Borborema Province (Caxito et al., 2016).

5.2. Ages, source and tectonic setting of the São Pedro Stock

LA-ICP-MS U-Pb zircon data for rocks of the São Pedro Stock indicate crystallization ages of 615 ± 2 Ma and 592 ± 22 Ma. Tonian zircon crystals that yielded an age of 981 ± 29 Ma are interpreted as inherited from previous formed crust, including material from the São Caetano Complex. A previous obtained ID-TIMS U-Pb zircon age for the

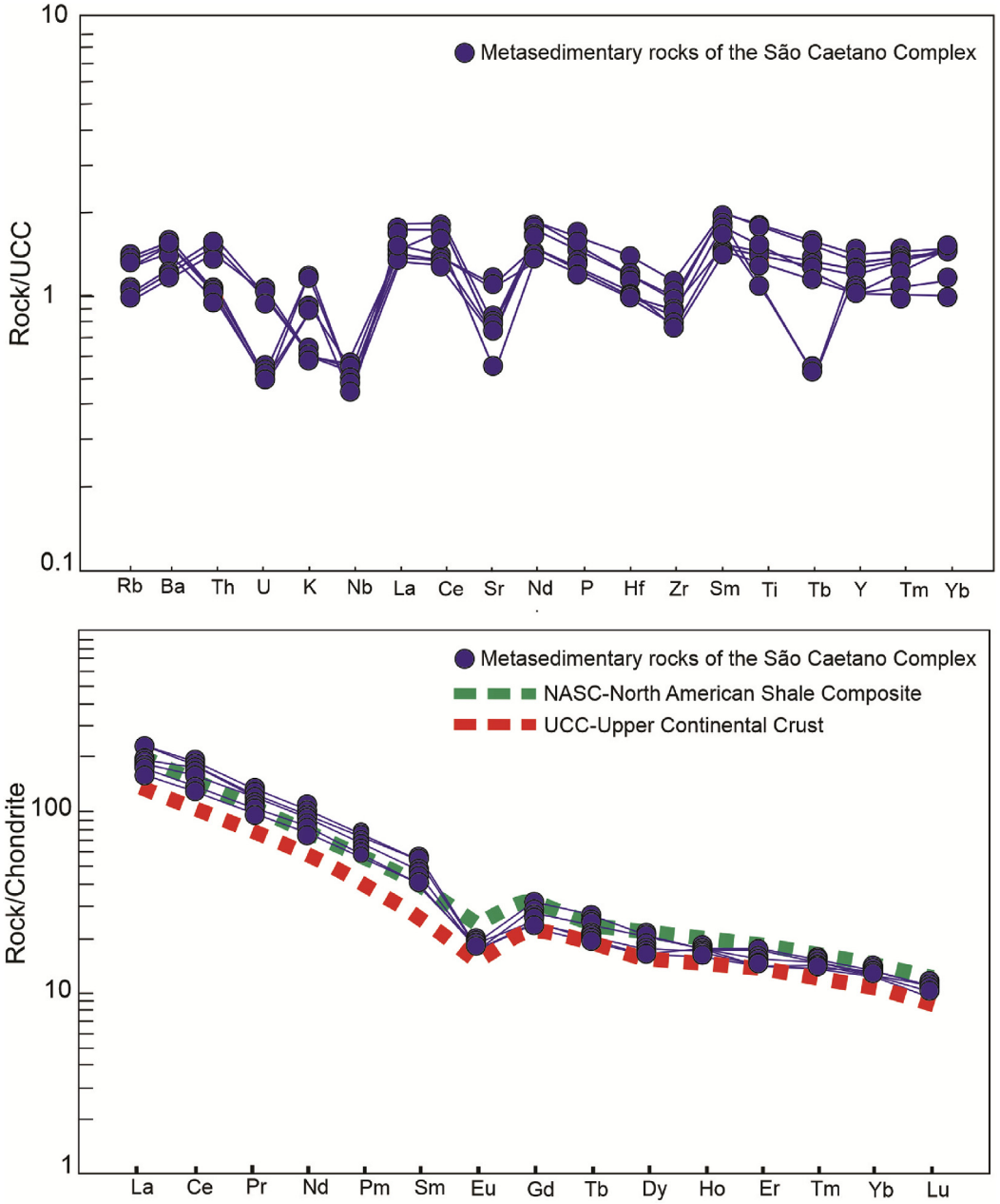

Fig. 9. São Caetano Complex: a) Spider diagram of trace element abundances; b) REE abundances. The data is compared with NASC and UCC from Haskin and Haskin (1966) and Rudnick and Gao (2003).

São Pedro Stock is quite similar to the oldest determinations (*i.e.* 948 ± 8 Ma, Santos, 1995). Based on the geochronological data of this study, this age might reflect crustal inheritance, lacking of Ediacaran grains or mixing of early and late Neoproterozoic zircon crystals. The absence of grains older than 1.0 Ga suggests limited or no Meso-Paleoproterozoic lithosphere interaction wih the magma during its ascent, which is common in other granitic domains of the Borborema Province (Sial and Ferreira, 2015).

The geochemical data suggest that the precursor magmas of the São Pedro stock share similarities with Cordilleran granites (Frost et al., 2001). Such features favor an origin involving mixing of juvenile magmas with differentiated and evolved continental crust, as also suggested by the Nd isotopic signature. Petrographic and geochemical data are compatible with I-type granites (*i.e.* modal hornblende, high amounts of Na_2O and CaO). Potential early Neoproterozoic igneous/metaigneous sources are widespread throughout the Central Subprovince, being collectively named as Cariris Velhos metagranites/orthogneisses (Santos et al., 2010; Van Schmus et al., 2011). However, the slightly peraluminous character as well as the presence of tiny muscovite crystals are indicative of contamination by aluminous crust during magma ascent (Chappel and White, 2001), possibly from the São Caetano Complex, the host sequence. Such interpretation is also supported by the similar Nd isotopic signature of both units, including T_{DM} model ages. Trace-element values are compatible with the presence of rutile, Ti-magnetite, sphene or amphiboles in the melt source, whereas REE signature might reflect the involvement of garnet in high-pressure deep-seated regions (Foley et al., 2000; Klemme et al., 2006).

The overall geochemical signature (high amounts of SiO_2, Al_2O_3, Na_2O and K_2O and LILE, low Nb, Ta, P and Ti) of the studied samples is compatible with magmas generated in convergent tectonic scenarios in later stages of subduction (Pearce, 1982, 1996; Barbarin, 1999). In such settings, magma generation occur in different crustal levels and involve

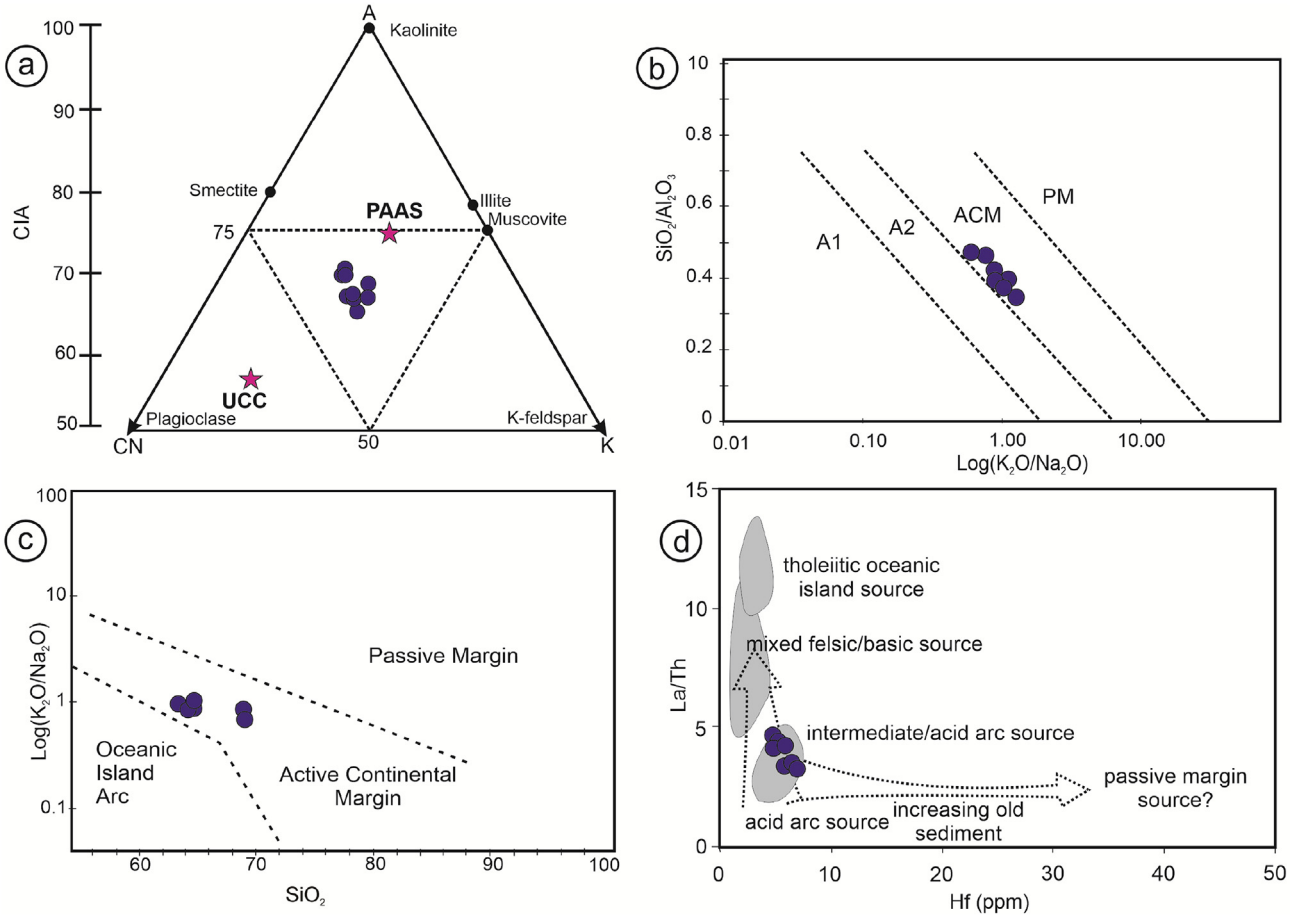

Fig. 10. Plots of the São Caetano Complex: a) $A(Al_2O_3) = CN(CaO + Na_2O)$ - $K(K_2O)$ ternary diagram of Nesbitt and Young (1982); b) $Log(K_2O/Na_2O)$ vs. SiO_2/Al_2O_3) diagram of Roser and Korsch (1988); c) SiO_2 vs. $Log(K_2O/Na_2O)$ diagram of Maynard et al. (1982); d) Hf vs. La/Th diagram of Floyd and Leveridge (1987). UCC and PAAS values are from Taylor and McLennan (1985). A1 = destritic sediments of andesitic and basaltic rocks deposited in oceanic island arcs. A2 = detritic sediments of felsic plutonic rocks deposited in oceanic island arcs. ACM = active continental margins. PM = Passive margins.

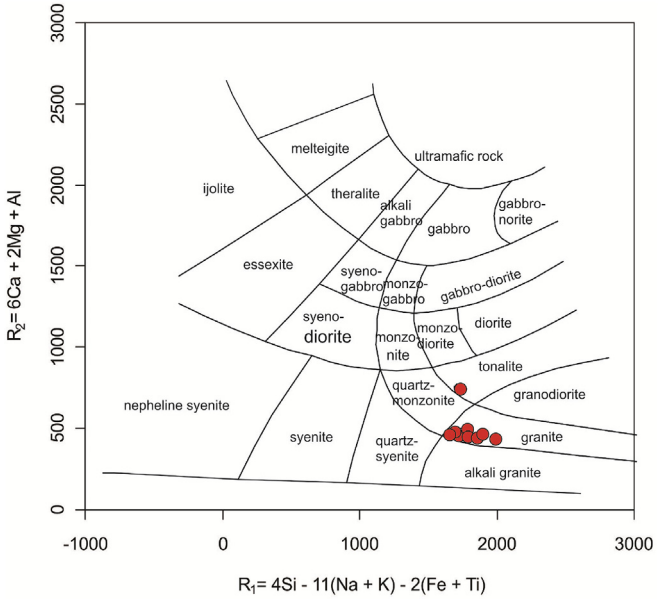

Fig. 11. Chemical-modal classification of studied samples of the São Pedro Stock on the R_1 vs. R_2 diagram (De la Roche et al., 1980).

variable degrees of partial melting (Gill, 2015). Two end-member petrogenetic processes may operate: a) hydrous melting of the upper mantle followed by fractional crystallization under H_2O saturated conditions (Grove et al., 2006) and, b) mixing of mafic and felsic material generating intermediate material (*i.e.* andesitic-dioritic magmas; Eichelberger et al., 2000, 2006). The absence of clear evidence of mafic rocks involvement in the source, including enclaves, xenoliths or mixing/mingling structures, suggest that mantle melting via solidus curve lowering is the likely mechanism of magma generation. Strong negative values of ε_{Nd} support the crustal character of the magma source, which can be triggered by AFC and/or incorporation of supracrustal material in the melt.

According to Guimarães et al. (2004, 2011), Brasiliano-related plutonism in the Central Subprovince is grouped as follows: a) classical calc-alkaline granites dated at 644-610 Ma; b) syn-kinematic high-K calc-alkaline and shoshonitic granites dated at 590-581 Ma; c) post collisional alkaline granites aged at 570 Ma; and, d) A-type granites dated at 540-512 Ma. The São Pedro stock crystallization ages lie in the transition between groups a) and b), representing pre-to syn-collisional granites, with strong crustal components in the source. The lack of major deformation markers within this stock, which is restricted to transcurrent movements only along its south border, suggest that there are no clear relationships between high temperature metamorphism and magma emplacement as interpreted in similar configurations throughout the province (Neves, 2012; Viegas et al., 2014). In summary, the São Pedro Stock represent one of a series of magmatic-arc related granites (see Brito Neves et al., 2016 for review) within the

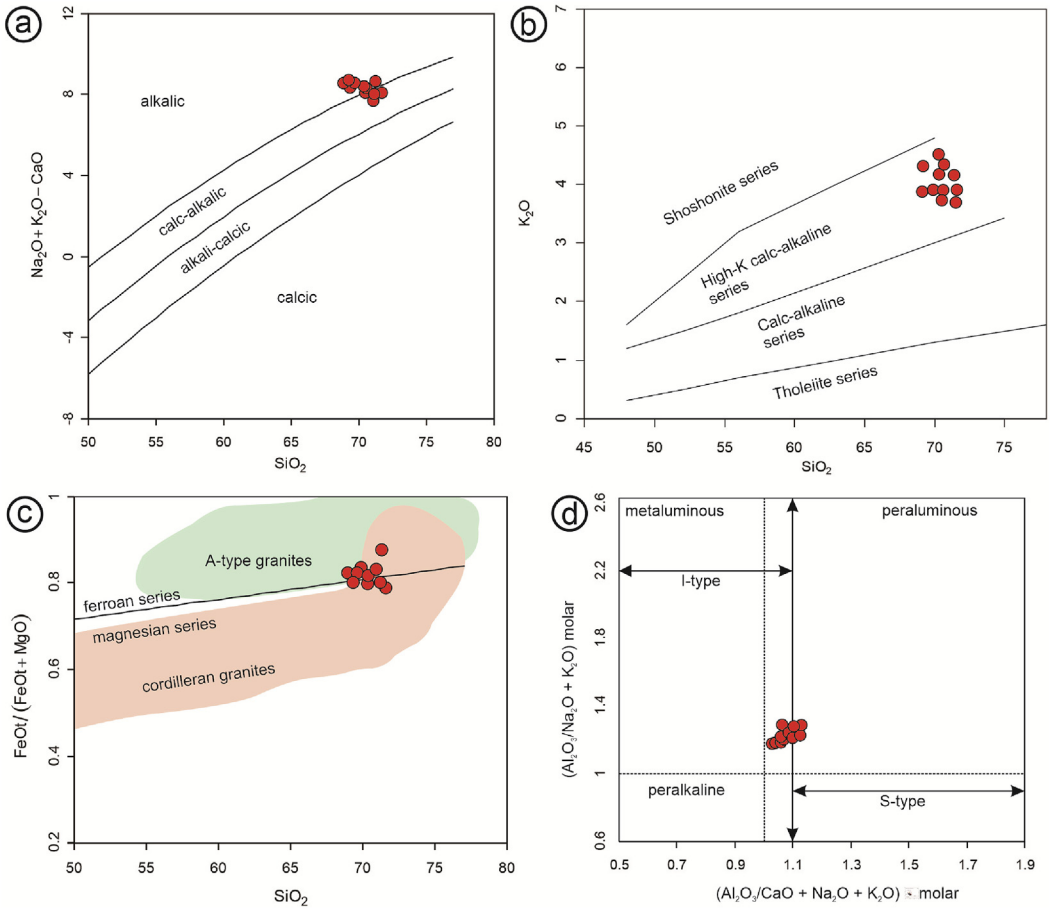

Fig. 12. Overall geochemical characteristics of major elements of the studied samples from the São Pedro Stock. a) SiO_2 vs. Na_2O + K_2O - CaO diagram (Frost et al. 2001); b) SiO_2 vs. K_2O diagram (Le Maitre et al. 1989); c) SiO_2 vs. FeOt/(FeOt/MgO) diagram (Frost et al., 2001); d) Al_2O_3/CaO + Na_2O + K_2O molar vs. Al_2O_3/(Na_2O + K_2O) molar diagram (modified by Maniar and Piccoli, 1989 and with the boundaries between I- and S-type granites from Chappell and White, 1992). Symbols are the same as Fig. 9.

central Borborema Province that intruded remnants of the early crust during a continental arc stage of the Brasiliano orogeny (Fig. 15c).

5.3. Correlations along West Gondwana

In spite of a younger maximum deposition age, correlative units to the São Caetano Complex are mainly present in the Central and Southern subprovinces of the Borborema Province. Marginal orogens bordering the São Francisco Craton record well known remnants of early Neoproterozoic orogenic crust, including the Riacho do Pontal (*i.e.* Afeição augen gneiss; Caxito et al., 2014a,b,c) and Sergipano fold belts (*i.e.* Marancó-Poço Redondo Domain metamorphic sequences; Carvalho, 2005; Oliveira et al., 2010). Cariris Velhos granites/orthogneisses interpreted as markers of crustal growth and reworking (*i.e.* Recanto, Riacho do Forno, Rocinha, Serra Negra and Flores) occur in the Central and Southern subprovinces and thus, can be interpreted as major sources for the sediments that filled the paleobasin of the São Caetano Complex (Kozuch, 2003; Santos et al., 2010; Guimarães et al., 2015).

The Brejo Seco and Paulistana complexes in the Riacho do Pontal Belt are interpreted as the result of post-convergence extension at 900-880 Ma (Caxito et al., 2016; Salgado et al., 2016), probably marking the first stages of an orogenic collapse phase, slightly similar to our younger obtained zircon age. In effect, Post-Cariris late Tonian and Cryogenian A-type granites, rift sequences and mafic-ultramafic intrusions of similar age are also found in the belts surrounding the northern São Francisco Craton margin, in the Rio Preto (Caxito et al., 2014c; Alcântara et al., 2017), Riacho do Pontal (Caxito et al., 2016; Salgado et al., 2016) and Sergipano (Oliveira et al., 2010) belts. In addition, zircon populations that range from 850 to 1000 Ma are present in several widespread Ediacaran metasedimentary and metavolcanosedimentary sequences throughout the province, such as the Araticum Complex of the Sergipano Fold Belt (Lima et al., 2019) and Cabrobró Complex of the Pernambuco-Alagoas Terrane (Cruz et al., 2014), also indicating inheritance of exhumed Stenian-Tonian crust.

In spite of well described Tonian arc-related units along Eastern Gondwana, such as granitic domains of the Mozambique Belt, marking an Andean-like subduction along the East African orogen (Archibald et al., 2017 and references therein), in West African domains, remnants of coeval sequences to the CVB are scarce. This is probably due to the overprinting of the Pan-African orogeny (630-530 Ma; Stern, 2002; Goscombe et al., 2017), with the exception to some cratonic sequences in the Congo, West Africa and Kalahari blocks (Kröner and Cordani, 2003; Oriolo et al., 2017) as well as their correlative cratons in South America (Fuck et al., 2008). However, a number of metasedimentary, metavolcanic and metaplutonic sequences within the Central African Fold Belt present Sm-Nd model ages (T_{DM}) that range from 1.0 to 1.6 Ga (Van Schmus et al., 2008), fitting with the obtained values for the São Caetano Complex, which implies a very similar crustal component between early Neoproterozoic sequences in NE South America and West Africa. The recognition of Tonian sequences derived from late Meso-to early Neoproterozoic arcs of Gondwana is of great importance for the record of early continental accretionary systems that are coeval to those from the Rodinia Supercontinent (Dalziel, 2000; Li et al., 2008).

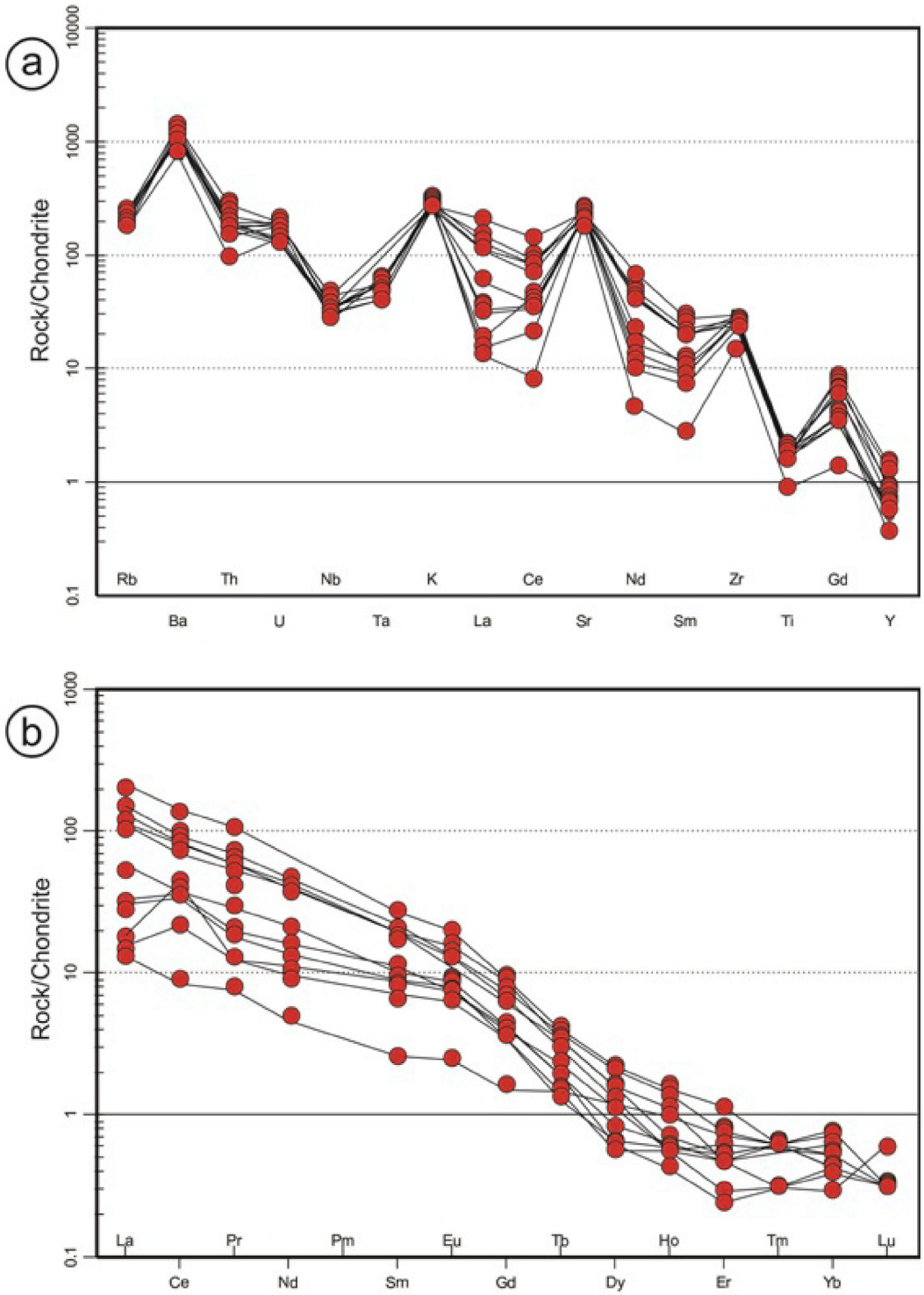

Fig. 13. São Pedro Stock: a) Spider diagram of trace element abundances; b) REE abundances normalized to the chondrite of Nakamura (1974).

Althought concrete correlations between west African sequences and those from the CVB are still speculative, remnants of ca. 900–990 Ma juvenile crust are present in the Saharan Metacraton (Küster et al., 2008), whilst metavolcanosedimentary sequences dated at ca. 1000-910 Ma are described in the West Congo Belt (Tack et al., 2001), that can be interpreted as the result of orogenic activity in the cratonic margins. Furthermore, basal sedimentary layers of the Bou-bouka Group of the Volta Basin and the Atacora unit of the Dahomey Belt present a number of zircon crystals that are partially coeval with the major age peak of the São Caetano Complex, representing possible chronocorrelated units (Clauer, 1976; Affaton et al., 1991; Carney et al., 2010; Ganade de Araújo et al., 2016).

On the other hand, the vast number of late Neoproterozoic granites of the Borborema Province, including those from the São Pedro Stock, constitute magmatic arc roots of the Brasiliano orogen, recording the final assembly stages of South America (Brito Neves et al., 2014). In spite of early Neoproterozoic arc-related juvenile magmatism recorded on the Tamboril Santa Quiteria Complex of the Northern Subprovince that spanned from 880 to 600 Ma (Arthaud et al., 2008; Ganade de Araújo et al., 2014b), in the Central Subprovince, Brasiliano-related

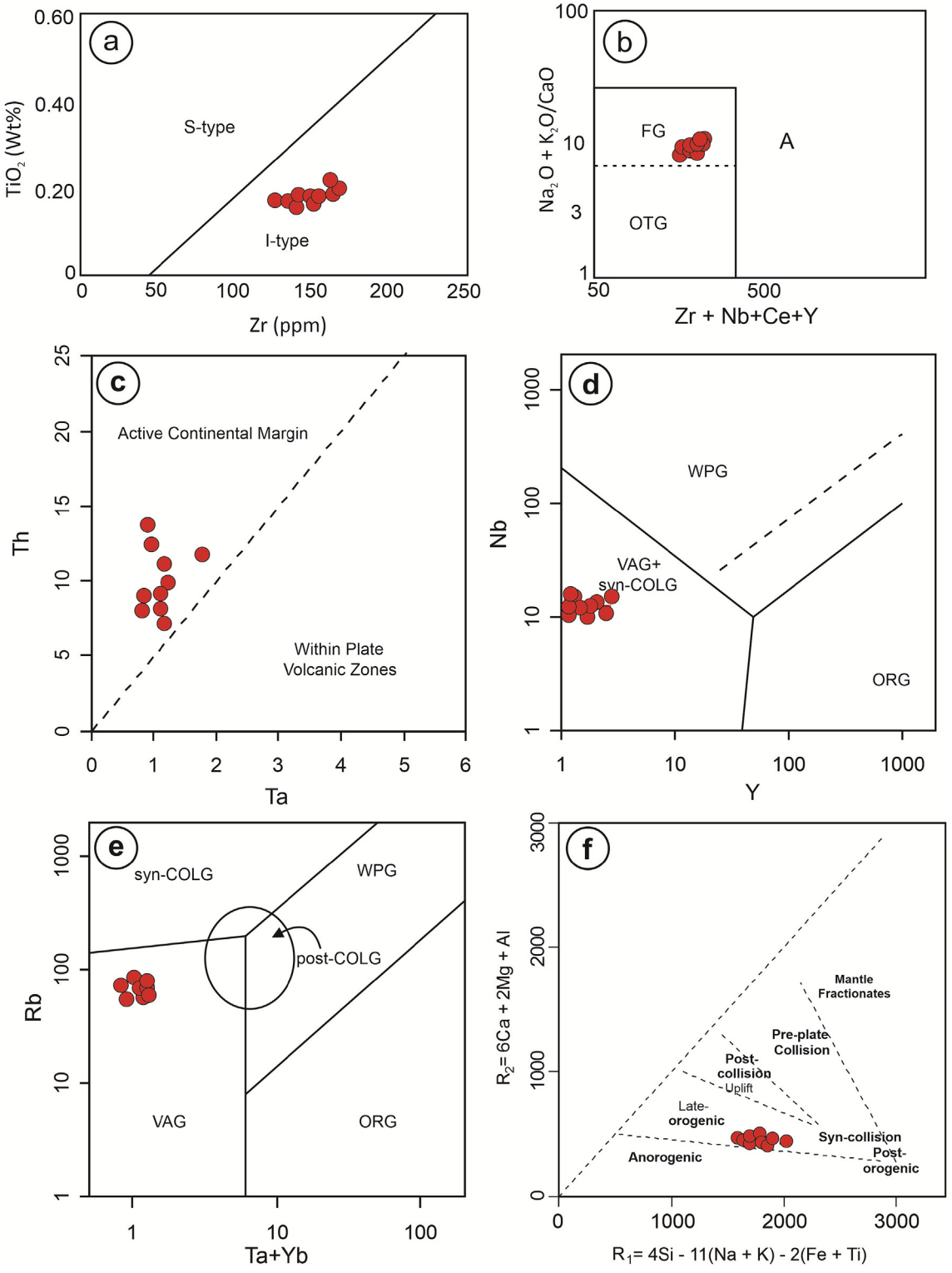

Fig. 14. Plots of the São Pedro Stock: a) Zr. Vs TiO_2 diagram with I and S fields from Chappell and White (1992); b) Zr + Nb + Ce + Y vs. (Na_2O + K_2O)/CaO from Whalen et al. (1987); c) Ta/Hf vs. Th/Hf plot of Schandl and Gorton (2002); d) Y vs. Nb and e) Ta + Yb vs. Rb of Pearce et al. (1984); f) R1 vs. R2 discriminant functions from Batchelor and Bowden (1985).

plutons that have emplaced between the late Neoproterozoic to Cambrian times, recorded on pre-, syn, and post-collisional episodes (Van Schmus et al., 2011). They mostly ranges from 635 to 580 Ma and have been recently interpreted as part of a 750 km long and up to 140 km wide Ediacaran continental magmatic arc (Brito Neves et al., 2016). Late collisional to post-orogenic magmatism is marked at around ca. 540-530 Ma (Hollanda et al., 2010).

Ediacaran to Cambrian granitic suites in Africa are widespread. For instance, correlative plutons to the São Pedro Stock are present in the Adamawa-Yaondé domain (Cameroon) of the Central African Belt, in which granites have occurred in the crust at the 630-620, 613-585 and 583-540 Ma intervals (Ngako et al., 2008 and references therein). Such

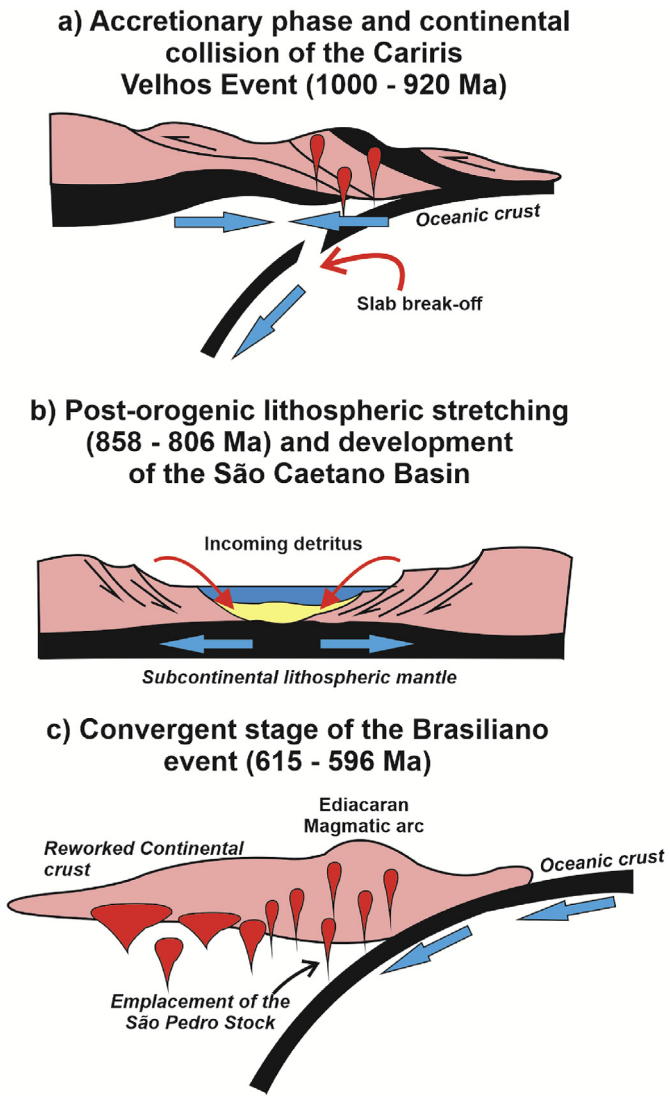

Fig. 15. Schematic illustration of the tectonic evolution of the Cariris Velhos Belt based on the obtained data. a) Accretionary-collisional phase of the early Neoproterozoic Cariris Velhos event; b) Post-orogenic within-plate stage and development of the São Caetano Basin; c) New subduction and voluminous granitic emplacement associated to the Brasiliano orogeny and crystallization of the São Pedro Stock.

stages are associated with protracted deformation and metamorphic events ranging from 620 to 540 Ma, being coeval to the crystallization of the São Pedro Stock, which is part of a number of described remnants of convergent tectonics that resulted from the West Gondwana assembly (Toteu et al., 2001, 2004; Owana et al., 2011).

6. Conclusions

Two distinct units of the CVB, Borborema Province support systematic tectonic overpriting during the Neoproterozoic in central West Gondwana. Detrital material ranging from 1.0 to 0.86 Ga is recorded in supracrustal rocks of the São Caetano Complex. These rocks are chemically similar to average models for continental crust and interpreted as exhumation products of the Cariris Velhos magmatic arc, but also incorporating a minor contribution from a Paleoproterozoic foreland, interpreted as the adjoining Paleoproterozoic Alto Moxotó Terrane. After a long period of systematic within-plate events with low rates of magma generation, the dominantly Tonian crust was intruded by granitic rocks, such as the Ediacaran São Pedro Stock, as well as other plutons within the CVB. Rocks from these stock present general characteristics that fit with continental-arc related I- to S type magmas (Cordilleran granites). Based on our investigation, we propose that multiple stages of convergent tectonics shaped this portion of the West Gondwana during the Neoproterozoic.

Acknowledgements

This work is part of the PhD thesis of Lauro Cézar M. de Lira Santos at UnB. The anonymous reviews comments are strongly appreciated. Elton L. Dantas and Fabrício A. Caxito are fellows of the Brazilian scientific council (CNPq, grants 308312/2014-7 and 454272/2014-6, respectively) and acknowledge for the received support. PAC acknowledges support from Australian Research Council grant FL160100168. We also thank INCT (Estudos tectônicos) for supporting this research project.

References

Affaton, P., Rahaman, M.A., Trompette, R., Sougy, J., 1991. The Dahomeyide orogen: tectonothermal evolution and relationships with the Volta basin. In: Dallmeyer, R.D., Lecorché, J. (Eds.), The West African Orogens and Circum-Atlantic Correlatives. Springer, New York, pp. 95–111.

Alcântara, D.C.B.G., Uhlein, A., Caxito, F.A., Dussin, I.A., Pedrosa-Soares, A.C., 2017. Stratigraphy, tectonics and detrital zircon U-Pb (LA-ICP-MS) geochronology of the Rio Preto Belt and northern Paramirim corridor, NE, Brazil. Braz. J. Genet. 47, 261–273. https://doi.org/10.1590/2317-4889201720160102.

Almeida, F.F.M., Hasui, Y., Brito Neves, B.B., Fuck, R.A., 1981. Brazilian structural provinces: an introduction. Earth Sci. Rev. 18, 1–29. https://doi.org/10.1016/0012-8252(81)90003-9.

Amorim, J.V.A., Guimarães, I., Farias, D.J.S., Lima, J.V., Santos, L., Ribeiro, B., Brinaer, C., 2018. Late-Neoproterozoic ferroan granitoids of the Transversal subprovince, Borborema Province, NE Brazil: petrogenesis and geodynamic implications. Int. Geol. Rev. 1–23. https://doi.org/10.1080/00206814.2018.1544936.

Archanjo, C.J., Hollanda, M.H.B.M., Rodrigues, S.W., Brito Neves, B.B., 2008. Fabrics of pre- and syntectonic granite plutons and chronology of shear zones in the Eastern Borborema Province, NE Brazil. J. Struct. Geol. 30, 310–336. https://doi.org/10.1016/j.jsg.2007.11.011.

Archibald, D.B., Collins, A.S., Foden, J.D., Payne, J.L., Macey, P.H., Holden, P., Razakamanana, T., 2017. Stenian-Tonian arc magmatism in west-central Madagascar: the genesis of the Dabolava Suite. J. Geol. Soc. 175, 111–129.

Arthaud, M.H., Caby, R., Fuck, R.A., Dantas, E.L., Parente, C.V., 2008. Geology of the northern Borborema Province, NE Brazil and its correlation with Nigeria, NW Africa. In: Pankhurst, R.J., Trouw, R.A.J., Brito Neves, B.B., De Wit, M.J. (Eds.), West Gondwana: Pre-Cenozoic correlations across the South Atlantic Region. Geological Society of London Special Publication, pp. 49–67.

Arthaud, M.H., Fuck, R., Dantas, E.L., Santos, T.J.S., Caby, R., Armstrong, R., 2015. The Neoproterozoic Ceará Group, Ceará Central domain, NE Brazil: deposition age and provenance of detritral material. New insights from U-Pb and Sm-Nd geochronology. J. South Am. Earth Sci. 58, 223–237. https://doi.org/10.1016/j.jsames.2014.09.007.

Barbarin, B., 1999. A review of the relationships between granitoid types, their origins and their geodynamic environments. Lithos 46, 605–626. https://doi.org/10.1016/S0024-4937(98)00085-1.

Basto, C.F., Caxito, F.A., Vale, J.A.R., Silveira, D.A., Rodrigues, J.B., Alkmim, A.R., Valeriano, C.M., Santos, E.J., 2019. An ediacaran Back-arc basin preserved in the transversal zone of the Borborema province: evidence from geochemistry, geochronology and isotope systematics of the ipueirinha group, NE Brazil. Precambrian Res. 320, 213–231. https://doi.org/10.1016/j.precamres.2018.11.002.

Batchelor, R.A., Bowden, P., 1985. Petrogenetic interpretation of granitoids series using multicationic parameters. Chem. Geol. 48, 43–55. https://doi.org/10.1016/0009-2541(85)90034-8.

Bathia, M.R., Crook, K.A.W., 1986. Trace element characteristics of graywackes and tectonic setting discrimination of sedimentary basis. Contrib. Mineral. Petrol. 92, 181–183. https://doi.org/10.1007/BF00375292.

Brito Neves, B.B., Van Schmus, W.R., Santos, E.J., Campos Neto, M.C., Kozuch, M., 1995. O Evento Cariris Velhos na Província Borborema: integração de dados, implicações e perspectivas. Rev. Bras. Geociencias 25, 279–296.

Brito Neves, B.B., Santos, E.J., Schmus, W.R.Q., 2000. Tectonic history of the Borborema province. In: Umberto Cordani; Edson José Milani; Antonio Thomaz Filho; Diogenes de Almeida Campos (Org.). Tectonic Evolution of South America. Rio de Janeiro: 31st International Geological Congress. Special Publication, pp. 151–182.

Brito Neves, B.B., Fuck, R.A., Pimentel, M.M., 2014. The Brasiliano collage in South America: a review. Braz. J. Genet. 44, 493–518. https://doi.org/10.5327/Z2317-4889201400030010.

Brito Neves, B.B., Santos, E.J., Fuck, R.A., Santos, L.C.M.L., 2016. A preserved early Ediacaran magmatic arc at the northernmost portion of the Transversal Zone central subprovince of the Borborema Province, Northeastern South America. Braz. J. Genet. 46, 491–508. https://doi.org/10.1590/2317-4889201620160004.

Brown, M., Johnson, T., 2018. Secular change in metamorphism and the onset of global plate tectonics. Am. Mineral. 103, 181–196. https://doi.org/10.2138/am-2018-6166.

Bühn, B.M., Pimentel, M.M., Matteini, M., Dantas, E.L., 2009. High spatial resolution analysis of Pb and U isotopes for geochronology by laser ablation multicollector inductively coupled plasma mass spectrometry (LA-MC-ICP-MS). Anais da Acadêmia Brasileira de Geociências 81, 1–16. https://doi.org/10.1590/S0001-37652009000100011.

Carney, J.N., Jordan, C.J., Thomas, C.W., Condon, D.J., Kemp, S.J., Duodo, J.A., 2010. Lithostratigraphy, sedimentation and evolution of the Volta Basin in Ghana. Precambrian Res. 183, 701–724. https://doi.org/10.1016/j.precamres.2010.08.012.

Carvalho, M.J., 2005. Evolução tectônica do domínio Marancó-Poço Redondo: Registro das orogêneses Cariris Velhos e Brasiliana na Faixa Sergipana, NE do Brasil. Universidade Estadual de Campinas, Campinas, pp. 192 (PhD thesis).

Cawood, A., Kroner, A., Collins, W.J., Kusky, T.M., Mooney, W.D., Windley, B.F., 2009. Accretionary orogens through Earth history. Geol. Soc. Lond. Specl. Publ. 318, 1–36. https://doi.org/10.1144/SP318.1.

Cawood, A., Hawkesworth, C.J., Dhuime, B., 2013. The continental record and the generation of continental crust. Geol. Soc. Am. Bull. 125, 14–32. https://doi.org/10.1130/B30722.1.

Caxito, F.A., Ulhein, A., Dantas, E.L., 2014a. The Afeição augen-gneiss suite and the record of the Cariris Velhos orogeny (1000-960 Ma) within the Riacho do Pontal Fold Belt, NE Brazil. J. South Am. Earth Sci. 51, 12–27. https://doi.org/10.1016/j.jsames.2013.12.012.

Caxito, F.A., Ulhein, A., Stevenson, R., Ulhein, G., 2014b. Neoproterozoic oceanic crust remmants in northeast Brazil. Geology 45, 387–390. https://doi.org/10.1130/G35479.1.

Caxito, F.A., Dantas, E.L., Stevenson, R., Uhlein, A., 2014c. Detrital zircon (U–Pb) and Sm–Nd isotope studies of the provenance and tectonic setting of basins related to collisional Orogens: the case of the Rio Preto fold belt on the northwest São Francisco Craton margin, NE Brazil. Gondwana Res. 26, 741–754. https://doi.org/10.1016/j.gr.2013.07.007.

Caxito, F.A., Uhlein, A., Dantas, E.L., Stevenson, R., Salgado, S.S., Dussin, I.A., Sial, A.N., 2016. A complete Wilson cycle recorded within the Riacho do Pontal orogen, NE Brazil: implications for the Neoproterozoic evolution of the Borborema province at the heart of West Gondwana. Precambrian Res. 282, 97–120. https://doi.org/10.1016/j.precamres.2016.07.001.

Chappel, B.W., White, A.J.R., 2001. Two contrasting granite types: 25 years later. Aust. J. Earth Sci. 48, 489–499. https://doi.org/10.1046/j.1440-0952.2001.00882.x.

Chappell, B.W., White, A.J.R., 1992. I- and S-types granites in Lachlan fold belt. Trans. R. Soc. Edinb. Earth Sci. 83, 1–26. https://doi.org/10.1017/S0263593300007720.

Clauer, N., 1976. Géochimie isotipique du strontium des milieux sédimentaires. Application à la géochronologie de la couverture du craton ouest-africain. Sciences Géologiques Strassburg, France, Mémoir 45 256 p.

Cordani, E.G., Pimentel, M.M., Aráujo, C.E.G., Fuck, R.A., 2013. The significance of the Transbrasiliano-Kandi tectonic corridor for the amalgamation of West Gondwana. Braz. J. Genet. 43, 583–597. https://doi.org/10.5327/Z2317-48892013000300012.

Costa, F.G., Palheta, E.S.M., Rodrigues, J.B., Gomes, I.G., Vasconcelos, A.M., 2015. Geochemistry and U-Pb zircon ages of plutonic rocks from the Algodões granite-greenstone terrane, troia Massif, northern Borborema province, Brazil: implications for paleoproterozoic subduction-accretion processes. J. South Am. Earth Sci. 59, 45–68. https://doi.org/10.1016/j.jsames.2015.01.007.

Costa, F.G., Klein, E.L., Lafon, J.M., MilhomemNeto, J.M., Galarza, M.A., Rodrigues, J.B., Naleto, J.L.C., Lima, R.G.C., 2018. Geochemistry and U–Pb–Hf zircon data for plutonic rocks of the Troia Massif, Borborema Province, NE Brazil: evidence for reworking of Archean and juvenile Paleoproterozoic crust during Rhyacian accretionary and collisional tectonics. Precambrian Res. 311, 167–194. https://doi.org/10.1016/j.precamres.2018.04.008.

Cruz, R.F., Pimentel, M.M., Accioly, A.C.A., 2014. Provenance of metasedimentary rocks of the western Pernambuco-Alagoas domain: contribution to understand the crustal evolution of southern Borborema province. J. South Am. Earth Sci. 56, 54–67.

Dalziel, I.W.D., Mosher, S., Gahagan, L.M., 2000. Laurentia-Kalahari collision and the assembly of Rodinia. J. Geol. 108, 499–513.

Dantas, E.L., Souza, Z.S., Wernick, E., Hackspacher, C., Martin, H., Xiadong, D., Li, J.W., 2013. Crustal growth in the 3.4-2.7 Ga São José do Campestre Massif, Borborema province, NE Brazil. Precambrian Res. 227, 12–156.

De la Roche, H., Leterrier, J., Grande Claude, P., Marchel, M., 1980. A classification of volcanic and plutonic rocks using R1–R2 diagrams and major element analyses – its relationship and current nomenclature. Chem. Geol. 29, 183–210.

De Wit, M.J., Brito Neves, B.B., Trouw, R.A.J., Pankhurst, R.J., 2008. Pre-Cenozoic correlations across the South Atlantic region: “the ties that bind”. In: Pankhurst, R.J., Trouw, R.A.J., Brito Neves, B.B., De Wit, M.J. (Eds.), West Gondwana: Pre-cenozoic Correlation across the South Atlantic Region. Geological Society, London, pp. 1–8.

DePaolo, D.J., 1981. A neodymium and strontium isotopic study of the Mesozoic calc-alkaline granitic batholiths of the Sierra Nevada and Peninsular Ranges, California. J. Geophys. Res. 86, 10470–10488.

Eichelberger, J.C., Chertkoff, D.G., Dreher, S.T., Nye, C.J., 2000. Magma in collision: rethinking chemical zonation in magma chambers. Geology 28, 603–628.

Eichelberger, J.C., Izbekov, E., Browne, B.L., 2006. Bulk chemical trends at arc volcanoes are not liquid lines of descent. Lithos 87, 135–154.

Fedo, C.M., Nesbitt, H.W., Young, G.M., 1995. Unraveling the effects of potassium metasomatism in sedimentary rocks and paleosols, with implications for paleo weathering conditions and provenance. Geology 23, 921–924.

Ferreira, Valley.J.W., Sial, A.N., Spicuzza, M., 2003. Oxygen isotope compositions and magmatic epidote from two contrasting metaluminous granitoids, NE Brazil. Contrib. Mineral. Petrol. 145, 205–216.

Fetter, A.H., Van Schmus, W.R., dos Santos, T.J.S., Arthaud, M., Nogueira Neto, J., Arthaud, M., 2000. U-Pb and Sm-Nd geochronological constraints on the crustal evolution and basement architecture of Ceara State, NW Borborema Province, NE Brazil: implications for the existence of the Paleoproterozoic supercontinent Atlantica. Rev. Bras. Geociencias 30, 102–106.

Floyd, A., Leveridge, B.E., 1987. Tectonic environment of the Devonian Gramscatho basin, south Cornwall: framework mode and geochemical evidence from turbiditic sandstones. Geol. Soc. Lond. Specl. Publ. 144, 531–542.

Foley, S.F., Barth, M.G., Jenner, G.A., 2000. Rutile/melt partition coefficient for trace elements and an assessment of the influence of rutile on the trace element characteristics of subduction zone magmas. Geochem. Cosmochim. Acta 64, 933–938.

Frost, B.R., Barnes, C.G., Collins, W.J., Arculus, R.J., Ellis, D.J., Frost, C.D., 2001. A geochemical classification of granitic rocks. J. Petrol. 42, 2033–2048.

Fuck, R.A., Brito Neves, B.B., Schobbenhaus, C., 2008. Rodinia descendants in South America. Precambrian Res. 160, 108–126.

Ganade de Araujo, C.E., Cordani, G.U., Weinberg, R., Basei, M.A.S., Armostrong, R., Sato, K., 2014a. Tracing Neoproterozoic subduction in the Borborema Province (NE-Brazil): clues from U-Pb geochronology and Sr-Nd-Hf-O isotopes on granitoids and migmatites. Lithos 202, 167–189.

Ganade de Araújo, C.E., Rubatto, D., Germann, J., Cordani, G.U., Caby, R., Basei, M.A.S., 2014b. Ediacaran 2,500-km-long synchronous deep continental subduction in the West Gondwana Orogen. Nat. Commun. 5, 5198.

Ganade de Araujo, C.E., Cordani, U.G., Agnossoumounde, Y., Caby, R., Basei, M.A.S., Weinberg, R.F., Sato, K., 2016. Tightening-up NE Brazil and NW Africa connections: New U-Pb/Lu–Hf zircon data of a complete plate tectonic cycle in the Dahomey belt of the West Gondwana Orogen in Togo and Benin. Precambrian Res. 276, 24–42.

Gerya, T., 2014. Precambrian geodynamics: concepts and models. Gondwana Res. 25, 442–463. https://doi.org/10.1016/j.gr.2012.11.008.

Gill, J., 2015. island arc volcanism, volcanic arcs. In: Harff, J., Meschede, M., Petersen, S., Thiede, J. (Eds.), Encyclopedia of Marine Geosciences. Springer, Dordrecht.

Gióia, S.M.C.L., Pimentel, M.M., 2000. The Sm-Nd isotopic method in the geocrhronology laboratory of the University of Brasilia. Anais da academia brasileira de ciências 72, 219–245.

Goscombe, B., Foster, D.A., Gray, D., Wade, B., Marsellos, A., Titus, J., 2017. Deformation correlations, stress field switches and evolution of an orogenic intersection: the Pan-African Kaoko Damara orogenic junction, Namibia. Geosci. Front. 8, 1187–1232.

Grove, T.L., Chatterjee, N., Parman, S.W., Médard, E., 2006. The influence of H_2O on mantle wedge melting. Earth Planet. Sci. Lett. 240, 74–89. https://doi.org/10.1016/j.epsl.2006.06.043.

Guimarães, I., Silva Filho, A.F., 2000. Evidence of multiple sources involved in the genesis of the Neoproterozoic Itapetim granitic complex, NE Brazil, based on geochemical and isotopic data. J. South Am. Earth Sci. 13, 561–586.

Guimarães, I.P., Silva Filho, A.F., Almeida, C.N., Van Schmus, W.R., Araújo, J.M.M., Melo, S.C., Melo, E.B., 2004. Brasiliano (Pan-African) granitic magmatism in the Pajeú-Paraíba belt, Northeast Brazil: Na isotopic and geochronological approach. Precambrian Res. 135, 23–53.

Guimarães, I., Silva Filho, A.F., Almeida, C.N., Macambira, M.B., Armstrong, R., 2011. U-Pb SHRIMP data constraints on calc-alkaline granitoids with 1.3-1.6 Ga Nd TDM model ages from central domain of the Borborema Province, NE Brazil. J. South Am. Earth Sci. 31, 383–396.

Guimarães, I., Van Schmus, W.R., Brito Neves, B.B., Bittar, S.M., Silva Filho, A.F., Armstrong, R., 2012. U Pb zircon ages of orthogneisses and supracrustal rocks of the CaririsVelhos belt: onset of Neoproterozoic rifting in the Borborema Province, NE Brazil. Precambrian Res. 192–195, 52–77.

Guimarães, I., Brito, M.F.L., Lages, G.A., Silva Filho, A.F., Santos, L., Brasilino, R.G., 2015. Tonian granitic magmatism of the Borborema Province, NE Brazil: a review. J. South Am. Earth Sci. 68, 97–112.

Haskin, M.A., Haskin, L.A., 1966. Rare earths in European shales: a redetermination. Science 154, 507–509.

Hine, R., WIlliams, I.S., Chappel, B.W., White, A.J.R., 1978. Contrasts between I- and S-type granitoids of the Kosciusko batholith. J. Geol. Soc. Aust. 25, 219–234.

Hollanda, M.H.B.M., Archanjo, C.J., Batista, J.R., Souza, L.C., 2015. Detrital zircon ages and Nd isotope compositions of the Seridó and Lavras da Mangabeira basins (Borborema Province, NE Brazil): evidence for exhumation and recycling associated with a major shift in sedimentary provenance. Precambrian Res. 258, 186–207.

Hollanda, M.H.B.M., Archanjo, C.J., Souza, L.C., Armstrong, R., Vasconcelos, P.M., 2010. Cambrian mafic to felsic mgmatism and its connections with transcurrent shear zones of the Borborema Province (NE Brasil): implications for the late assembly of the West Godwana. Precambrian Res. 178, 1–14.

Jackson, S.E., Pearson, N.J., Griffin, W.L., Belousova, E.A., 2004. The application of laser ablation-inductively coupled plasma-mass spectrometry to in situ U-Pb zircon geochronology. Chem. Geol. 211, 47–69.

Jöns, N., Schenk, V., 2008. Relics of the Mozambique Ocean in the central East African Orogen: evidence from the Vohibory Block of southern Madagascar. J. Metamorphic Geol. 26, 17–28.

Keskin, M., 2003. Magma generation by slab steepening and breakoff beneath subduction-accretion complex: an alternative model for collision-related volcanism in Eastern Anatolia, Turkey. Geophys. Res. Lett. 30, 1–4.

Klemme, S., Gunther, D., Hametner, K., Prowatke, S., Zack, T., 2006. The partitioning of trace elements between ilmenite, ulvospinel, armalcolite and silicate melts with implications for the early differentiation of the moon. Chem. Geol. 234, 251–263.

Kozuch, M., 2003. Isotopic and Trace Element Geochemistry of Early Neoproterozoic Gneissic and Metavolcanic Rocks in the CaririsVelhos Orogen of the Borborema Province, Brazil, and Their Bearing Tectonic Setting. PhD thesis. Kansas University, Lawrence, pp. 199.

Kröner, A., Cordani, U.G., 2003. African, southern Indian and South American cratons were not part of the Rodinia supercontinent: evidence from field relationships and geochronology. Tectonophysics 375, 325–352.

Küster, D., Liégeois, J., Matukov, D., Sergeev, S., Lucassen, F., 2008. Zircon

geochronology and Sr, Nd, Pb isotope geochemistry of granitoids from Bayuda Desert and Sabaloka (Sudan): evidence for a Bayudian event (920–900 Ma) preceding the Pan-African orogenic cycle (860–590 Ma) at the eastern boundary of the SaharanMetacrat. Precambrian Res. 164, 16–39.
Lages, G.A., Dantas, E.L., 2016. Floresta and Bodocó Mafic-Ultramafic Complexes, western Borborema Province, Brazil: geochemical and isotope constraints for evolution of a Neoproterozoic arc environment and retroeclogitic hosted Ti-mineralization. Precambrian Res. 280, 95–119.
A classification of igneous rocks and glossary of terms. In: Le Maitre, R.W., Bateman, Dubek, A., Keller, J., Lameyre, J., Le Bas, M.J., Sabine, A., Schmid, R., Sørensen, H., Streckeisen, A., Woolley, A.R., Zanettin, B. (Eds.), Recommendations of the International Union of Geological Sciences Subcommission on the Systematics of Igneous Rocks. Blackwell, Oxford, pp. 193.
Li, Z.X., Bogdanova, S.V., Collins, A.S., Davidson, A., De Waele, B., Ernst, R.E., Fitzsimons, I.C.W., Fuck, R.A., Gladkochub, D., Jacobs, J., Karlstrom, K.E., Lu, S., Natapov, L.M., Pease, Pisarevsky, S.A., Thrane, K., Vernikovsky, 2008. Assembly, configuration, and break-up history of Rodinia: a synthesis. Precambrian Res. 160, 179–210.
Li, Z.H., Gerya, T.V., Burg, J., 2010. Influence on tectonic overpressure on P-T paths of HP-UHP rocks in continental collisionl zones: thermocechanical modeling. J. Metamorph. Petrol. 28, 227–247.
Lima, H.M., Pimentel, M.M., Fuck, R.A., Santos, L.C.M.L., Dantas, E.L., 2019. Geochemical and detrital zircon geochronological investigation of the metavolcanosedimentaryAraticum complex, sergipano fold belt: implications for the evolution of the Borborema Province, NE Brazil. J. South Am. Earth Sci. 86, 176–192.
Ludwig, K.R., 2012. Isoplot/Ex Version 4: A Geochronological Tollkit for Microsoft Excel. Geochronology Center, Berkeley.
Lugmair, G.W., Marti, K., Scheinin, N.B., 1978. Incomplete mixing products from r-, p-, and s-process nucleosynthesis: Sm-Nd systematics in Allend inclusion Ek 1-04-1. Lunar and Planetary Science, vol. IX. Lunar Science Institute, Houston, Texas, pp. 672–674.
Madsen, J.K., Thorkelson, D.J., Friedman, R.M., Marshall, D.D., 2006. Cenozoic to recent configurations in the Pacific basin: ridge subduction and slab windowmagmatism in western North America. Geosphere 2. https://doi.org/10.1130/GES00020.1.
Maniar, D., Piccoli, M., 1989. Tectonic discrimination of granitoids. Geol. Soc. Am. Bull. 101, 635–643.
Matteinni, M., Junges, S.L., Dantas, E.L., Pimentel, M.M., Buhn, B.M., 2009. In situ zircon U-Pb and Lu-Hf isotope systematic on magmatic rocks: insights on the crustal evolution of the Neoproterozoic Goiás Magmatic Arc, Brasília belt, Central Brazil. Gondwana Reearch 16, 200–212.
Maynard, J.B., Valloni, R., Yu, H., 1982. Composition of modern deep-sea sands from arc related basins. In: In: Legget, J.K. (Ed.), Trench-forearc Geology: Sedimentation and Tectonics on Modern and Ancient Active Plate Margins, vol. 10. Geological Society of London Special Publication, pp. 551–561.
Nakamura, N., 1974. Determination of REE, Ba, Fe, Mg, Na and K in carbonaceous and ordinary chondrites. Geochem. Cosmochim. Acta 38, 757–775.
Nascimento, M.A.L., Galindo, A.C., Medeiros, C., 2015. Ediacaran to Cambrian magmatic suites in the Rio Grande do Norte domain, extreme northeastern Borborema province (NE of Brazil): current knowledge. J. South Am. Earth Sci. 58, 281–299.
Nesbitt, H.W., Young, G.M., 1982. Early Proterozoic climates and plate motions inferred from major element chemistry of lutites. Nature 299, 715–717.
Neves, S., 2003. Proterozoic history of the Borborema province (NE Brazil): correlations with neighboring cratons and Pan-African belts and implications for the evolution of western Gondwana. Tectonics 22, 1031.
Neves, S., 2015. Constraints from zircon geochronology on the tectonic evolution of the Borborema Province (NE Brazil): widespread intracontinental Neoproterozoic reworking of a Paleoproterozoic accreationary orogeny. J. South Am. Earth Sci. 58, 150–164.
Neves, S., Mariano, G., Correia, B., Silva, J.M.R., 2003. 70 m.y. of synorogenic plutonism in eastern Borborema Province (NE Brazil): temporal and kinematic constraints on the Brasiliano Orogeny. Geodin. Acta 19, 213–236.
Neves, S., da Silva, J.M.R., Bruguier, O., 2017. Geometry, kinematics and geochronology of the Sertânia Complex (central Borborema Province, NE Brazil): Assessing the role of accretionary versus intraplate processes during West Gondwana assembly. Precambrian Res. 298, 552–571. https://doi.org/10.1016/j.precamres.2017.07.006.
Ngako, V., Affaton, P., Njonfang, E., 2008. Pan-African tectonics in northwestern Cameroon: implication for the history of western Gondwana. Gondwana Res. 14, 509–522.
Oliveira, R.G., Medeiros, W.E., 2018. Deep crustal framework of the Borborema Province, NE Brazil, derived from gravity and magnetic data. Precambrian Res. 315, 45–65.
Oliveira, E.P., Windley, B.F., Araújo, M.N.C., 2010. The Neoproterozoic Sergipano orogenic belt, NE Brazil: a complete plate tectonic cycle in western Gondwana. Precambrian Res. 181, 64–84.
Oliveira, E.P., McNaughton, N., Windley, B.F., Carvalho, M.J., Nascimento, R.S., 2015. Detrital zircon U–Pb geochronology and whole-rock Nd-isotope constraints on sediment provenance in the Neoproterozoic Sergipano orogen, Brazil: from early passive margins to late foreland basins. Tectonophysics 662, 183–194.
Oriolo, S., Oyhantçabal, P., Wemmer, K., Siegesmund, S., 2017. Contemporaneous assembly of Western Gondwana and Final Rodinia break-up: Implications for the supercontinent cycle. Geosci. Front. 8, 1431–1445.
Owana, S., Schultz, B., Lothar, R., MvondoOndoa, J., Ekodeck, G.E., Tchoua, F.M., Affaton, P., 2011. Pan-African metamorphic evolution in the southerYounde Group (oubanguide Complex, Cameroon) as revealed by EMP-monazite dating and thermobarometry of garnet metapelites. J. Afr. Earth Sci. 59, 125–139. https://doi.org/10.1016/j.jafrearsci.2010.09.003.
Padilha, A.L., Vitorello, Í., Pádua, M.B., Fuck, R.A., 2016. Deep magnetotelluric signatures of the early Neoproterozoic CaririsVelhos tectonic event within the Transversal sub-province of the Borborema Province, NE Brazil. Precambrian Res. 275, 7–83.
Pearce, J.A., 1982. Trace elements characteristics of lavas from destructive plate boundaries. In: Thorpe, R.S. (Ed.), Andesites. John Wiley and Sons, London, pp. 525–548.
Pearce, J.A., 1996. Sources and settings of granitic rocks. Episodes 19, 120–125.
Pearce, J.A., Harris, N.B.W., Tindle, A.G., 1984. Trace element discrimination diagrams for the tectonic interpretation of granitic rocks. J. Petrol. 24, 956–983.
Roser, B., Korsch, R.J., 1988. Provenance signatures of sandstone-mudstone suites determined using discriminant function analysis of major-element data. Chem. Geol. 67, 119–139.
Rudnick, R.L., Gao, S., 2003. Composition of the continental crust. In: Holland, H.D., Turekian, K.K. (Eds.), Treatise on Geochemistry 3. Elsevier, Amsterdam, pp. 1–64.
Salgado, S.S., Ferreira Filho, C.F., Caxito, F.A., Uhlein, A., Dantas, E.L., Ross, S., 2016. The Ni-Cu-PGE mineralized BrejoSeco mafic-ultramafic layered intrusion, Riacho do Pontal Orogen: onset of Tonian (ca. 900 Ma) continental rifting in Northeast Brazil. J. South Am. Earth Sci. 70, 324–339.
Santos, E.J., 1995. O complexo granítico Lagoa das Pedras: acresção e colisão na região de Floresta (Pernambuco), Província Borborema (PhD thesis). Instituto de Geociências da Universidade de São Paulo, São Paulo, pp. 228.
Santos, E.J., Medeiros, V.C., 1999. Constraints from granitic plutonism on proterozoic crustal growth of the Transverse Zone, Borborema Province, NE-Brazil. Rev. Bras. Geociencias 29, 73–84.
Santos, E.J., Nutman, A., Brito Neves, B.B., 2004. Idades SHRIMP U-Pb do Complexo Sertânia: implicações sobre a evolução tectônica da Zona Transversal, Província Borborema. Geol. Usp. Série Científica 4, 1–12.
Santos, E.J., Van Schmus, W.R., Kozuch, M., Brito Neves, B.B., 2010. The Cariris Velhos tectonic event in northeast Brazil. J. South Am. Earth Sci. 29, 61–76.
Santos, L.C.M.L., Dantas, E.L., Santos, E.J., Santos, R.V., Lima, H.M., 2015a. Early to late Paleoproterozoic magmatism in NE Brazil: the Alto Moxoto Terrane and its tectonic implications for the pre-West Gondwana assembly. J. South Am. Earth Sci. 58, 188–209.
Santos, T.J.S., Amaral, W.S., Ancelmi, M.F., Pitarello, M.Z., Fuck, R.A., Dantas, E.L., 2015b. U-Pb age of the coesite-bearing eclogite from NW Borborema Province, NE Brazil: implications for western Gondwana assembly. Gondwana Res. 28, 1183–1196.
Santos, L.C.M.L., Dantas, E.L., Vidotti, R.M., Cawood, A., Santos, E.J., Fuck, R.A., Lima, H.M., 2017a. Two-stage terrane assembly in Western Gondwana: insights from structural geology and geophysical data of central Borborema Province, NE Brazil. J. Struct. Geol. 103, 167–184. https://doi.org/10.1016/j.jsg.2017.09.012.
Santos, L.C.M.L., Dantas, E.L., Cawood, P.A., Santos, E.J., Fuck, R.A., 2017b. Neoarchean crustal growth and Paleoproterozoic reworking in the Borborema Province, NE Brazil: insights from geochemical and isotopic data of TTG and metagranitic rocks of the Alto Moxotó Terrane. J. South Am. Earth Sci. 79, 342–363. https://doi.org/10.1016/j.jsames.2017.08.013.
Santos, L.C.M.L., Dantas, E.L., Cawood, A., Lages, G.d.A., Lima, H.M., Santos, E.J., 2018. Accretion tectonics in western Gondwana deduced from Sm-Nd isotope mapping of terranes in the Borborema Province, NE Brazil. Tectonics 37, 2727–2743. https://doi.org/10.1029/2018TC005130.
Schandl, E.S., Gorton, M., 2002. Application of high field strength elements to discriminate tectonic settings in VMS environments. Econ. Geol. 97, 629–642.
Sdrolias, M., Muller, R.D., 2006. Controls on back-arc basin formations. Geochem. Geophys. Geosyst. 7, 1–40. https://doi.org/10.1029/2005GC001090.
Sial, A.N., Ferreira, V.P., 2015. Magma associations in Ediacaran granitoids of the Cachoeirinha-Salgueiro and Alto Pajeú terranes, northeastern Brazil: Forty years of studies. J. South Am. Earth Sci. 68, 1–21.
Sizova, E., Gerya, T., Brown, M., Perchuk, L.L., 2010. Subduction styles in the Precambrian: insight from numerical experiments. Lithos 116, 209–229. https://doi.org/10.1016/j.lithos.2009.05.028.
Stern, R.A., 1997. The GSC sensitive high resolution ion microprobe (SHRIMP): analytical techniques of zircon U-Th-Pb age determinations and performance evaluation. In: radiogenic age and isotopic studies: Report 10. Geol. Survey Canada Curr. Res. 1–31.
Stern, R.J., 2002. Crustal evolution in the East African Orogen: a neodymium isotopic perspective. J. Afr. Earth Sci. 34, 109–117. https://doi.org/10.1016/S0899-5362(02)00012-X.
Stern, R.J., 2005. Evidence from ophiolites, blueschists, and ultrahigh-pressure metamorphic terranes that the modern episode of subduction tectonics began in Neoproterozoic time. Geology 33, 557–560. http://doi:10.1130/g21365.1.
Streckeisen, A.L., 1976. To each plutonic rocks its proper name. Earth Sci. Rev. 12, 1–33.
Tack, L., Wingate, M.T.D., Liégois, J., Fernander-Alonson, M., Beblond, A., 2001. Early Neoproterozoic magmatism (1000-910 Ma) of the Zandnian and Mayumbian groups (Bas-Congo): onset of Rodinia rifting at the western edge of the Congo craton. Precambrian Res. 110, 227–306.
Tatsumi, Y., 2005. The subduction factory: how it operates on Earth. GSA Today 15, 4–10.
Tatsumi, Y., Kogiso, T., 2003. The subduction factory: its role in the evolution of the Earth's crust and mantle. Geol. Soc. Lond. Specl. Publ. 219, 55–80.
Taylor, S.R., McLennan, S.M., 1985. The Continental Crust; its Composition and Evolution. Blackwell, Oxford, pp. 132.
Thompson, R.N., 1982. Magmatism of the British terciary volcanic province. Scott. J. Geol. 18, 50–107.
Toteu, F., Van Schmus, W.R., Penaye, J., Michard, A., 2001. New U-Pb, and Sm-Nd data from North-Central Cameroon and its bearing on the pre-Pan-African history of Central Africa. Precambrian Res. 108, 45–73.
Toteu, S.f., Penaye, J., Poudjondjomani, Y., 2004. Geodynamic evolution of the Pan-African belt in central Africa with special reference to Cameroon. Can. J. Earth Sci. 41, 73–85.
Van Schmus, W.R., Brito Neves, B.B., Hackspacher, C., Babinski, M., 1995. U/Pb and Sm/

Nd geochronologic studies of the eastern Borborema Province, Northeast Brazil: initial conclusions. J. South Am. Earth Sci. 8, 267–288.
Van Schmus, W.R., Brito Neves, B.B., Williams, I.S., Hackspacher, C., Fetter, A.H., Dantas, E.L., Babinski, M., 2003. The Seridó Group of NE Brazil, a late Neoproterozoic pre- to syn-collisional basin in West Gondwana: insights from SHRIMP U-Pb detrital zircon ages and Sm-Nd crustal residence (TDM) ages. Precambrian Res. 127, 287–327.
Van Schmus, W.R., Oliveira, E., Silva Filho, A.F., Toteu, F., Penaye, J., Guimarães, I., 2008. Proterozoic links between the Borborema province, NE Brazil, and the central African Fold belt. Geol. Soc. Lond. Specl. Publ. 294, 66–69.
Van Schmus, W.R., Kozuch, M., Brito Neves, B.B., 2011. Precambrian history of the Zona transversal of the Borborema province, NE Brazil: insights from Sm/Nd and U/Pb geochronology. J. South Am. Earth Sci. 31, 227–252.
Viegas, L.G., Archanjo, C.J., Hollanda, M.H.B.M., Vauchez, A., 2014. Microfabrics and zircon U-Pb (SHRIMP) chronology of mylonites from the Patos shear zone (Borborema Province, NE Brazil). Precambrian Res. 243, 1–17.
Viegas, L.G., Menegon, L., Archanjo, C.J., 2016. Brittle grain-size reduction of feldspar, phase mixing and strain localization in granitoids at mid-crustal conditions (Pernambuco shear zone, NE Brazil). Solid Earth 7, 375–396.
Wang, W., Cawood, A., Pandit, M.K., Zhou, M.-F., Chen, W.-T., 2017. Zircon U–Pb age and Hf isotope evidence for an Eoarchaean crustal remnant and episodic crustal reworking in response to supercontinent cycles in NW India. J. Geol. Soc. 174, 759–772. https://doi.org/10.1144/jgs2016-080.
Whalen, J.B., Curie, K.L., Chappel, B.W., 1987. A-type granites: geochemical characteristics, discrimination and petrogenesis. Contrib. Min. Petrol. 95, 407–419.